

Analysis of Mineral Trapping for CO₂ Disposal in Deep Aquifers

Tianfu Xu, John A. Apps, and Karsten Pruess

Earth Sciences Division, Lawrence Berkeley National Laboratory, University of
California, Berkeley, CA 94720.

Abstract. CO₂ disposal into deep aquifers has been suggested as a potential means whereby atmospheric emissions of greenhouse gases may be reduced. However, our knowledge of the geohydrology, geochemistry, geophysics, and geomechanics of CO₂ disposal must be refined if this technology is to be implemented safely, efficiently, and predictably. As a prelude to a fully coupled treatment of physical and chemical effects of CO₂ injection, we have analyzed the impact of CO₂ immobilization through carbonate precipitation. A survey of all major classes of rock-forming minerals, whose alteration would lead to carbonate precipitation, indicated that very few minerals are present in sufficient quantities in aquifer host rocks to permit significant sequestration of CO₂. We performed batch reaction modeling of the geochemical evolution of three different aquifer mineralogies in the presence of CO₂ at high pressure. Our modeling considered (1) redox processes that could be important in deep subsurface environments, (2) the presence of organic matter, (3) the kinetics of chemical interactions between the host rock minerals and the aqueous phase, and (4) CO₂ solubility dependence on pressure, temperature and salinity of the system. The geochemical evolution under both natural background and CO₂ injection conditions was evaluated. In addition, changes in porosity were monitored during the simulations. Results indicate that CO₂ sequestration by matrix minerals varies considerably with rock type. Under favorable conditions the amount of CO₂ that may be sequestered by precipitation of secondary carbonates is comparable with and can be larger than the effect of CO₂ dissolution in pore waters. The precipitation of ankerite and siderite is sensitive to the rate of reduction of ferric mineral precursors such as glauconite, which in turn is dependent on the reactivity of associated organic material. The accumulation of carbonates in the rock matrix and induced rock mineral alteration due to the presence of dissolved CO₂ lead to a considerable decrease in porosity. The numerical experiments described here provide useful insight into sequestration mechanisms, and their controlling geochemical conditions and parameters.

1. Introduction

A reduction in the release rate of carbon dioxide (CO₂) to the atmosphere is considered an essential first step in the control of global warming. One way of achieving this is to dispose of CO₂ into structural reservoirs in deep permeable geologic formations, (Holloway, 1997). Such formations could include aquifers, oil and gas fields, and coal seams. Aquifers are the most abundant fluid reservoirs in the subsurface, and are commonly present beneath power plants throughout the world. The deepest aquifers in the United States usually contain brackish or saline water. Aquifers exceeding 10,000 ppm (TDS: total dissolved solids) are excluded by the U.S. Environmental Protection Agency as underground sources of drinking water. Hence, they are logical targets for the eventual disposal of CO₂. The feasibility of storing CO₂ in aquifers has been discussed several times in the technical literature over the last decade. These include an evaluation of the feasibility of CO₂ aquifer storage in The Netherlands (Lohuis, 1993) and in the Alberta Basin, Canada (Gunter et al., 1993, Bachu et al., 1994, Law and Bachu, 1996, Gunter et al., 1996 and 1997). Furthermore, large-scale CO₂ disposal in an aquifer is already being practiced in the Norwegian sector of the North Sea (Korbol and Kaddour, 1995).

The long-term CO₂ sequestration raises new scientific challenges (Rudnicki and Wawersik, 1999), particularly in the fields of geohydrology, geochemistry, geophysics, and geomechanics. These challenges must be addressed before this technology can be implemented safely, efficiently, and predictably. In this paper, we focus our attention on geochemical issues arising from the aquifer disposal.

Carbon dioxide is retained in geologic formations in three ways (Hitchon, 1996). First, CO₂ can be trapped as a gas or supercritical fluid under a low-permeability caprock. This process, commonly called hydrodynamic trapping, will likely be, in the short term, the most important method of retention. Second, CO₂ can dissolve into the groundwater, referred to as a solubility trapping. The dissolution of CO₂ in groundwater increases the acidity of water and affects the solubilities of minerals composing the host rock matrix. Third, CO₂ can react directly or indirectly with minerals and organic matter in the geologic formation leading to the precipitation of secondary carbonates and the

solubilization of organic matter. The former process, so-called ‘mineral trapping’, is potentially attractive because it could immobilize CO₂ for long time scales, and prevent its easy return to the atmosphere. The interaction of CO₂ with alkaline aluminosilicate minerals will also result in the formation of soluble carbonates and bicarbonates in solution, thereby enhancing “solubility trapping”.

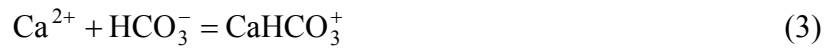
The chemical reactions induced by CO₂ injection are as follows (Ortoleva et al., 1998). First, CO₂ dissolves in water to produce the weak carbonic acid:



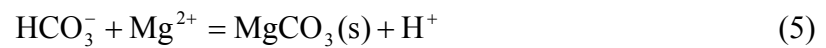
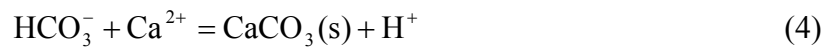
This is followed by rapid dissociation of carbonic acid to form the bicarbonate ion:



The increased acidity induces dissolution of many of the primary host rock minerals, which in turn causes complexing of dissolved cations with the bicarbonate ion such as



The dissolved bicarbonate species react with divalent cations to precipitate carbonates. Formation of calcium, magnesium, and ferrous carbonates are expected to be the primary means by which CO₂ is immobilized (Gunter et al., 1997).



Investigators have long recognized that CO₂ can be extracted from the atmosphere by silicate weathering and subsequent deposition of carbonate minerals (Lasaga, 1981).

The appealing concept that CO₂ could be permanently sequestered as carbonates in the subsurface environment by “mineral trapping” (Bachu et al., 1994) has prompted experimental studies in Europe (Pearce et al., 1996; Rochelle et al., 1996) and Canada (Gunter et al., 1997) to investigate this process. The European studies were carried out using reservoir sandstones and supercritical CO₂ at temperatures of 105 and 80°C and CO₂ pressures of 90 and 200 bars, respectively, in autoclaves for periods of from 1 to 8 months. The most notable observations were significant alteration of pre-existing calcite and dolomite, alteration of anhydrite with concomitant precipitation of calcite, and somewhat tenuous evidence for the corrosion of detrital feldspar and coupled precipitation of smectite-Na when in the presence of seawater.

The Canadian experiments were performed using samples from a glauconitic sandstone aquifer in the Alberta Sedimentary Basin, a potential candidate for CO₂ disposal, in an attempt to validate results obtained with a batch geochemical model. Because the kinetics of silicate reactions at room temperature are too slow to observe any significant CO₂ consumption in a reasonable length of time, experiments were performed for one month at 105 °C at 90 bars CO₂ pressure to accelerate the reaction rate. The experimental results indicate that little CO₂ was trapped through reaction with aluminosilicate minerals on this time scale. The reactions that were observed involved the rapid dissolution of carbonate minerals. The geochemical model predicted that from 6 to 40 years were required for the experiments to come to equilibrium. Extending the model to the field, it was found by these Canadian investigators that the CO₂ trapping reactions would take hundreds of years to complete after the formation water had equilibrated at the temperature of the aquifer (54 °C) and at the proposed injection CO₂ pressure (260 bar). However, they did indicate that the reaction could be fast enough to form effective CO₂ traps given the tens- to hundreds-of-thousands of years residence time of fluids in the deep aquifers. The long residence time should ensure that any CO₂ mineral trapping would be complete before any CO₂ impregnated fluid would break through at the earth's surface.

Numerical modeling of geochemical processes is a necessary tool for long-term CO₂ disposal in deep aquifers, because alteration of the predominant host rock aluminosilicate minerals is very slow and is not experimentally accessible under ambient deep-aquifer conditions. Because the range of rock mineralogy in geologic formations is very broad, we present geochemical modeling analyses for the interaction of CO₂ fluid at pressure with three different rock types using the code TOUGHREACT (Xu and Pruess, 1998). Our initial simulations employed a glauconitic sandstone aquifer from the Alberta Sedimentary Basin, which has been studied previously by Gunter et al. (1997). In their simulations, annite was used as a substitute for glauconite, which is the ferrous iron end-member of the biotite mica series. Glauconite is a mica, which is distinguished by a substantial amount of K in the interlayer positions and a high concentration of Fe³⁺ in the octahedral sheet. In contrast, annite is the Fe²⁺ end member component of the phlogopite-annite mica series, which contains no Fe³⁺. Use of annite as a substitute for glauconite overestimates the amount of siderite (FeCO₃) precipitation, and hence the extent of CO₂ sequestration. In the present study, the model mineral assemblage was modified to more closely reflect that expected in a glauconitic sandstone. We also assumed that organic matter, represented by the generic composition CH₂O, was present in the glauconitic sandstone. This allowed us to consider processes involving redox sensitive pairs such as Fe³⁺/Fe²⁺, CO₂(aq)/CH₄(aq), H₂O(aq)/H₂(aq) and SO₄²⁻/HS⁻. The geochemical evolution for both the natural system and that involving CO₂ injection was simulated. The CO₂ sequestration capacity of both aqueous and mineral phases was evaluated. Changes in porosity due to mineral dissolution and precipitation were also monitored.

The second rock type evaluated, was a proxy for a sediment from the United States Gulf Coast (Apps, 1996). The mineralogy is similar to that commonly encountered in sedimentary basins, although our model host rock contained significantly less inert quartz than is usual for such sediments. Gulf Coast Mesozoic and Tertiary sediments were buried rapidly and incorporated significant amounts of organic matter. Maturation of the organic matter into petroleum and natural gas, and its migration into numerous structural traps characterizes these sediments. Another feature of relevance is the entrapment of evaporite salt beds during sedimentary accumulation.

The third rock type we investigated was dunite, an essentially monomineralic rock consisting of olivine. This rock is a mantle residue after depletion of basaltic magma, and occurs rarely at the earth's surface. However, it has a very large CO₂ sequestration capacity (see Appendix B). Olivine is a binary solid solution of the pure end-member minerals, forsterite (Mg₂SiO₄) and fayalite (Fe₂SiO₄). The modeling method and processes considered for the last two types of rock are similar to those of the glauconitic sandstone case.

After reporting results of our model simulations involving the three types of rock, we discuss the following important issues: (1) a comparison of the simulated mineral assemblage with field observation, (2) the extent to which CO₂ may be sequestered by secondary carbonates, (3) changes in porosity due to rock mineral alteration, (4) the time required for sequestration, (5) limitations of geochemical modeling, and (6) the effects of physical processes on geochemistry. Finally, we present several conclusions from the geochemical modeling analysis for CO₂ disposal in deep aquifers.

2. Glauconitic sandstone

2.1 Problem setup

Gunter et al. (1997) modeled the geochemistry of CO₂ injection in a glauconitic sandstone aquifer in the Alberta Sedimentary Basin, Canada (a potential candidate for CO₂ disposal). The glauconitic sandstone aquifer is a medium- to fine-grained litharenite. The average mineral composition is 87% quartz, 2% potassium-feldspar, 1% plagioclase, 5% glauconite, 2% kaolinite, 1% calcite, 1% dolomite, and 1% siderite. The average porosity is 12%. Gunter et al. (1997) modeled water-rock reactions driven by the formation of carbonic acid when CO₂ is injected into deep aquifers using PATHARC.94 (Perkins and Gunter, 1995). In their simulations, the CO₂ injection pressure was set at 260 bar. Annite was used as a substitute for glauconite. Plagioclase was simulated by assuming the presence of discrete fractions of end member components, anorthite and albite. In the present study, we initially assumed the same mineralogy as Gunter et al. (1997). Our analyses were carried out using the code TOUGHREACT (Xu and Pruess, 1998). TOUGHREACT is a multiphase non-isothermal reactive geochemical transport program, the main features of which are presented in Appendix C. In order to compare

our results with those of Gunter et al. (1997), we only used the batch geochemical modeling features of TOUGHREACT. In the future, the geochemical modeling results will be coupled with the fluid flow features of TOUGHREACT. Our parallel simulation shows that annite is rapidly destroyed with precipitation of siderite (FeCO_3), the later being the principal mineral trap for CO_2 . A maximum of about 40 kg of CO_2 per m^3 of host rock medium can be sequestered in mineral phases. Our results are similar to those of Gunter et al. (1997).

The use of annite as a substitute for glauconite overestimates the availability of Fe^{2+} , the amount of siderite (FeCO_3) precipitation, and hence the degree of CO_2 sequestration. Glauconite is a mica, which is distinguished by a substantial amount of K in the interlayer positions and a high concentration of Fe^{3+} in the octahedral sheet. In contrast, annite is the trioctahedral ferrous iron (Fe^{2+}) end member component ($\text{KFe}_3\text{AlSi}_3\text{O}_{10}(\text{OH})_2$) of the phlogopite-annite mica series, which contains no Fe^{3+} . In the present study, the model mineral assemblage was modified to more closely reflect that expected in a glauconitic sandstone. Thus, we estimated a representative glauconite chemical composition and thermodynamic properties from descriptions of the mineralogical compositions of glauconite and its paragenesis as reported in the published literature, described in Appendix A. We also incorporated oligoclase as a solid solution of plagioclase, and calculated the thermodynamic properties of oligoclase from calorimetric studies of plagioclase solid solutions reported in the literature (also given in Appendix A). Furthermore, we assumed that organic matter, represented by the generic composition, CH_2O , was present in the glauconitic sandstone. The decomposition of organic matter is a complex process. A more realistic representation of organic matter should be investigated in the future. Also, instead of using muscovite as a proxy for illite, we assumed that illite was actually present as a primary mineral. We believe the modified mineralogy more accurately represents the natural condition. In our modeling, we consider redox sensitive couples such as $\text{Fe}^{3+}/\text{Fe}^{2+}$, $\text{CO}_2(\text{aq})/\text{CH}_4(\text{aq})$, $\text{H}_2\text{O}(\text{aq})/\text{H}_2(\text{aq})$, and $\text{SO}_4^{2-}/\text{HS}^-$, which are very important in the geochemical evolution of sedimentary basins.

The initial mineral abundances used in the present modeling (Table 2.1, expressed as the volume fraction of the entire medium), are based on the previous work (Hitchon,

1996, p. 138), but with the addition of a 2.64% volume fraction of organic matter. Organic matter is commonly found in sedimentary basins. The primary mineral dissolution is considered to be kinetically controlled. The rate law used is given in Eq. C.1 (in Appendix C) using two exponential parameters μ and n set equal to one (i.e., first order kinetics). Rate constants at any given temperature are calculated from Eq. C.2, and kinetic constant at 25 °C (k_{25}) and activation energy (E_a). These kinetic parameters are also given in Table 2.1. Some kinetic parameters were taken directly from published scientific literature. The references are listed in the last column of Table 2.1. Others were set to or modified from minerals with known kinetic properties. Precipitation of possible secondary minerals (Table 2.1 with initial $V_f = 0$ where V_f is mineral volume fraction) is represented using the same kinetic rate expression as that for dissolution. However, precipitation can differ in several respects, as nucleation, Ostwald ripening, crystal growth processes, and reactive surface areas must be taken into account in some circumstances (Plummer et al., 1978; Steefel and van Capellen, 1990). To simplify the description of precipitation kinetics, the precipitation kinetic constant for a secondary mineral is assumed to be one order of magnitude greater than its corresponding dissolution rate constant. Note that all rate constants in Table 2.1 (including secondary phases) are for dissolution. Because the rate constants assumed for precipitation reactions are larger than those for dissolution, formation of secondary minerals occurs effectively at conditions close to local equilibrium. A total surface area of 10 m²/dm³ medium was used. The initial surface area of each primary mineral (Table 2.1) is calculated from its volume fraction multiplied by the total surface area. With time, the surface areas change in complex ways. In this study, however, we simply relate the surface areas of the primary minerals at some time to the mineral volume fraction by

$$A = A^0 \frac{V_f}{V_f^0} \quad (7)$$

where A , and V_f are the reactive surface area and volume fraction of a primary mineral, respectively, and superscript zero indicates the values at time $t = 0$. With the exception of the clay minerals, the reactive surface areas for secondary minerals are set to 0.25 m²/dm³

at all times. Surface areas for illite, kaolinite, smectite-Na, and smectite-Ca are increased by two orders of magnitude, as this area corresponds to the actual predicted geometric surface area based on the assumption that the particles are in the range of 0.1 to 1 μm in diameter and 0.01 – 0.1 μm thick. The surface area for glauconite is increased by only one order of magnitude, because authigenic glauconite is usually more coarsely crystalline than other clay minerals, as it is commonly observed in crystallites up to 10 μm in diameter. Because estimates of field reactive surface areas cover a wide range of values (Nordstrom and Alpers, 1997), we performed several simulations to analyze the sensitivity of the rate of CO_2 sequestration to the reactive surface area.

Table 2.1. List of initial mineral volume fractions, potential secondary mineral phases, and their kinetic properties. All rate constants are listed for dissolution. The constants for precipitation are increased correspondingly by one order of magnitude.

Mineral	Chemical composition	Volume (%)	Surface area (m^2/dm^3 medium)	k_{25} (moles $\text{m}^{-2}\text{s}^{-1}$)	E_a (KJ/mol)	Reference
Primary:						
quartz	SiO_2	71.28	7.128	1.2589×10^{-14}	87.50	Tester et al. (1994)
K-feldspar	KAlSi_3O_8	1.76	0.176	1.00×10^{-12}	67.83	Blum and Stillings (1995)
kaolinite	$\text{Al}_2\text{Si}_2\text{O}_5(\text{OH})_4$	1.76	0.176×10^2	1.00×10^{-13}	62.76	Nagy (1995)
calcite	CaCO_3	0.88	0.088	1.60×10^{-9}	41.87	Svensson and Dreybrodt (1992)
dolomite	$\text{CaMg}(\text{CO}_3)_2$	0.88	0.088	0.60×10^{-9}	41.87	assigned based on calcite
siderite	FeCO_3	0.88	0.088	0.60×10^{-9}	41.87	assigned based on calcite
illite	$\text{K}_{0.6}\text{Mg}_{0.25}\text{Al}_{1.8}(\text{Al}_{0.5}\text{Si}_{3.5}\text{O}_{10})(\text{OH})_2$	2.64	0.264×10^2	1.00×10^{-14}	58.62	Knauss and Wolery (1989)
glauconite	$\text{K}_{1.5}\text{Mg}_{0.5}\text{Fe}_{2.5}\text{Fe}_{0.5}\text{AlSi}_{7.5}\text{O}_{20}(\text{OH})_2$	4.4	0.440×10	1.00×10^{-14}	58.62	set to illite
organic	CH_2O	2.64	0.264	1.00×10^{-13}	0.0	assigned based on kaolinite
oligoclase	$\text{CaNa}_4\text{Al}_6\text{Si}_{14}\text{O}_{40}$	0.88	0.088	1.00×10^{-12}	67.83	set to K-feldspar
porosity	-----	12				
total	-----	100				
Secondary:						
albite-low	$\text{NaAlSi}_3\text{O}_8$	0.0	0.25	1.00×10^{-12}	67.83	Blum and Stillings (1995)
smectite-Na	$\text{Na}_{0.290}\text{Mg}_{0.26}\text{Al}_{1.77}\text{Si}_{3.97}\text{O}_{10}(\text{OH})_2$	0.0	0.25×10^2	1.00×10^{-14}	58.62	set to illite
smectite-Ca	$\text{Ca}_{0.145}\text{Mg}_{0.26}\text{Al}_{1.77}\text{Si}_{3.97}\text{O}_{10}(\text{OH})_2$	0.0	0.25×10^2	1.00×10^{-14}	58.62	set to illite

Most solubility products for minerals were taken from the EQ3/6 V7.2b database (Wolery, 1992) that were derived from thermodynamic data using SUPCRT92 (Johnson et al., 1992), except for glauconite, oligoclase, and organic matter (see Appendix A).

Two simulations were performed. The first simulation was for water-rock interaction under natural conditions without CO_2 injection, here called the “background case”. The second simulation considers a CO_2 injection pressure of 260 bar. This pressure

is the same as that chosen by Gunter et al. (1997) for the glauconitic sandstone aquifer, and is based on the assumption that the aquifer is 1500 m deep, and can sustain CO₂ disposal injection pressures of that magnitude. In the present simulation, the CO₂ gas pressure is assumed to be in equilibrium with the solution at all times. Thus, the CO₂ gas is treated as an exterior boundary condition with a constant pressure. The solubility of CO₂ in the aqueous phase depends on pressure, temperature, and salinity. The detailed formulation for these factors in our model is given in Appendix D.

The geochemical simulations consider 1 m³ water-saturated medium. The initial condition used in the simulation is a pure 1.0 M solution of sodium chloride reacting with the primary minerals listed in Table 2.1 at a temperature of 54°C, a pH of 7, and an Eh of -0.1 V. Reactant phases are those minerals initially present in the aquifer formation. The reactant minerals dissolve progressively into the formation water, thus modifying the water composition and leading to precipitation of product phases, with sequestration of CO₂ upon precipitate of carbonates.

2.2. Results

Background without CO₂ injection

The evolution of pH and Eh is presented in Figure 2.1. At about 4000 years, a pH minimum of 6.7 occurs. The values of Eh move in the opposite direction, and the Eh maximum corresponds to the minimum in pH. After 12000 years, an approximately constant pH of 7 and a Eh of -0.16 V are achieved. Both CO₂ and CH₄ are generated at different periods during the simulations. In the present simulations, we consider only the aqueous CO₂ and CH₄ species. However, we calculated the corresponding gaseous partial pressures indirectly. Take CH₄ as an example, CH₄(g) = CH₄(aq). The mass-action equation for equilibrium is presented in Eq. (D.1) in Appendix D. By setting the CH₄ gaseous fugacity coefficient and the aqueous activity coefficient equal to one, CH₄ partial pressure can be approximately calculated by

$$P_{CH_4} = C_{CH_4} / K_{CH_4} \quad (8)$$

where P is the partial pressure (bar), C is the aqueous concentration (mol/kg H_2O), and K is the equilibrium constant. The gas partial pressures calculated from Eq. (8) are presented in Figure 2.2. The highest CO_2 partial pressure occurs at the lowest value of pH, i.e., the location of CO_2 partial pressure maximum value is consistent with that of pH minimum. After 10000 years, CH_4 appears and CO_2 disappears. The distribution of mineral abundances is presented in Figure 2.3. Oligoclase and kaolinite dissolve completely after 4000 years, the location is coincident with that of the pH minimum (Figure 2.1a). Organic matter dissolves at a constant rate. Glauconite initially dissolves faster at lower pH values, but eventually slows to a constant rate after 12000 years. The change in dissolution rate is consistent with the appearance of CH_4 (Figure 2.2b). Illite precipitates initially (before 4000 years), but dissolves after the disappearance of kaolinite. Albite-low and smectite-Na generally precipitate. K-feldspar initially dissolves, and then precipitates. Calcite and siderite precipitate in minor amounts. Dolomite initially dissolves, and then precipitates. Porosity (Figure 2.4) generally decreases due mainly to precipitation of smectite-Na that has a lower density and larger volume than the reactant minerals.

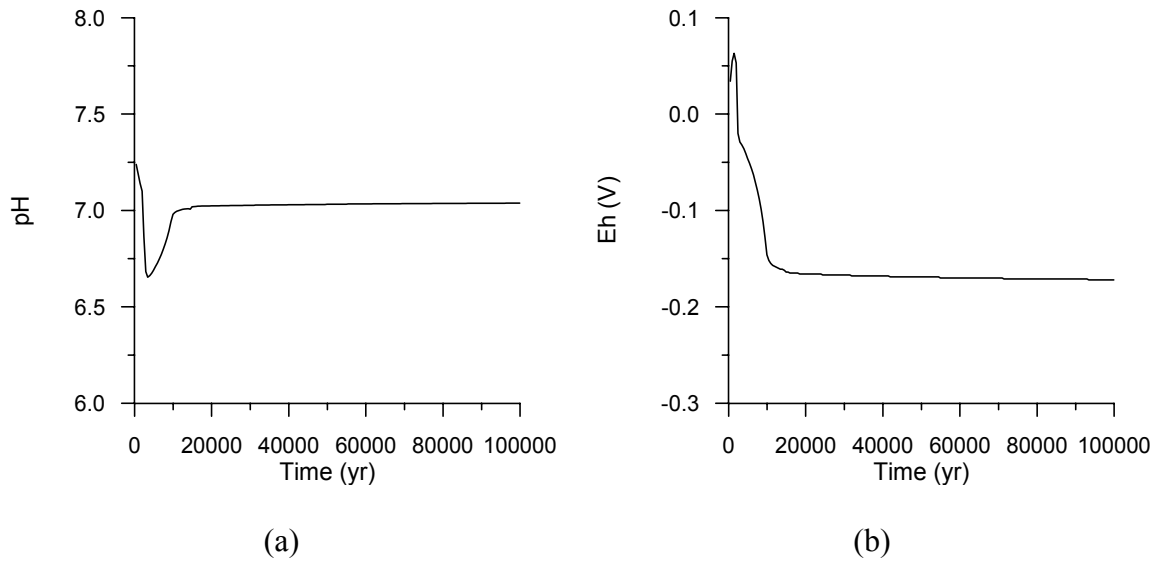


Figure 2.1. Evolution of pH and Eh obtained for the glauconitic sandstone case (without CO₂ injection).

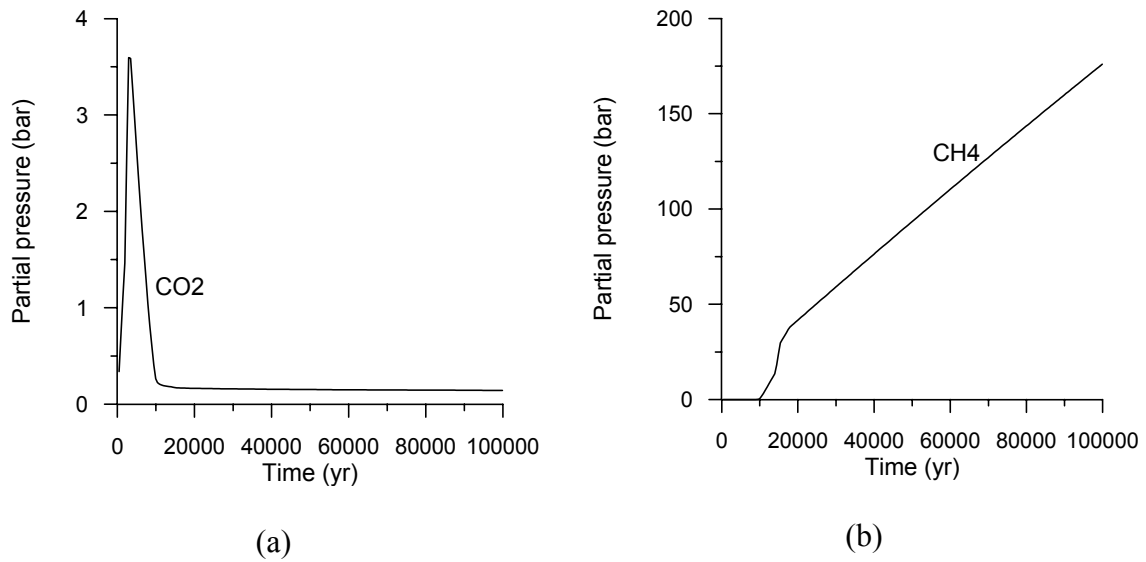


Figure 2.2. Distribution of gas partial pressures obtained for the glauconitic sandstone case (without CO₂ injection).

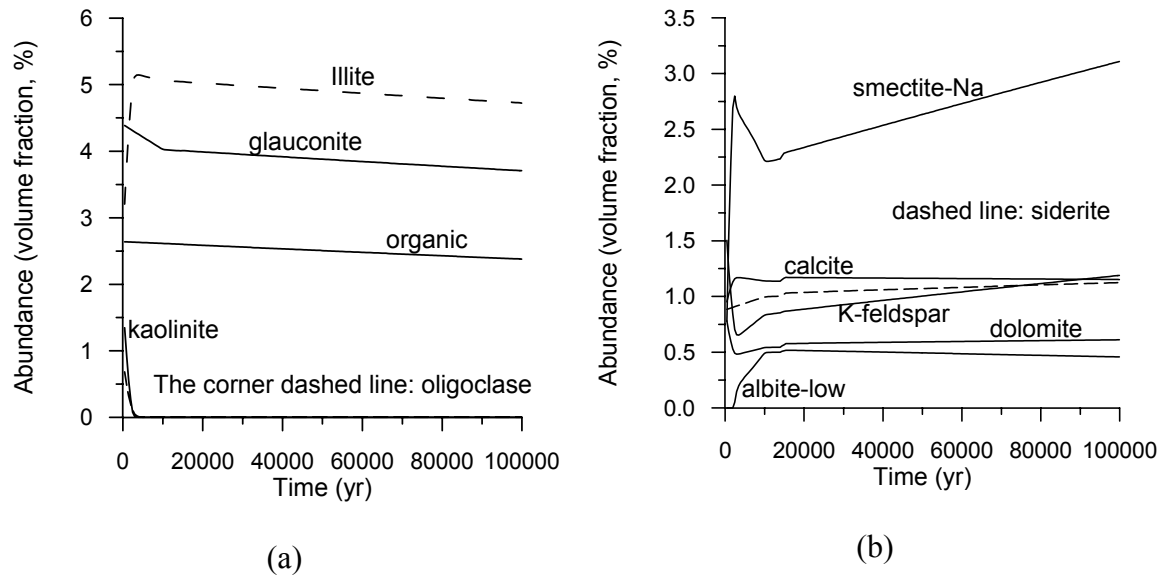


Figure 2.3. Distribution of mineral abundances for the glauconitic sandstone case (without CO₂ injection).

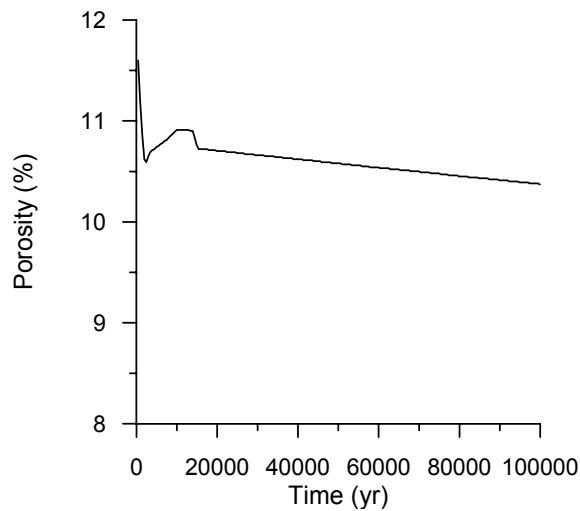


Figure 2.4. Porosity evolution for the glauconitic sandstone case (without CO₂ injection).

With CO₂ injection

With the instantaneous imposition of a constant CO₂ pressure of 260 bar on the formation water, an abrupt change of water composition occurs. With time, the reactant minerals dissolve and secondary mineral phases precipitate, and eventually, the formation

water saturates with respect to the latter. Compared with the background case, a lower pH (Figure 2.5a) and higher Eh (Figure 2.5b) are obtained with CO₂ injection, both of which are buffered by the CO₂ gas pressure. CH₄ generation is suppressed because of the higher values of Eh. The distribution of mineral phases is presented in Figure 2.6. The mineral assemblages are generally similar to those without CO₂ injection (compare Figure 2.6 to 2.3). However, a CO₂ injection pressure of 260 bar significantly enhances mineral dissolution and precipitation processes because of the decreased pH. Consequently, glauconite and illite dissolve at much higher rates (compare Figure 2.6a to Figure 2.3a). Organic matter dissolves at the same rate as the previous simulation, because equilibrium is not achievable and the rate expression remains essentially constant (see Appendix A and Eq C.1 in Appendix C).

Calcite and dolomite precipitate to a limited extent (Figure 2.6b), as with the previous simulation without CO₂. However, siderite precipitation is significantly greater than that with the previous simulation, because of greater availability of carbonate and more rapid glauconite dissolution. Greater precipitation of K-feldspar and smectite-Na can also be observed. Some of the CO₂ is immobilized by precipitation of three carbonate minerals, calcite, dolomite, and siderite. The cumulative sequestration of CO₂ with time is presented in Figure 2.7. Most CO₂ is sequestered through siderite (FeCO₃) precipitation (Figure 2.6b), but only minor quantities of CO₂ are sequestered through calcite and dolomite precipitation, because both minerals are more soluble than siderite in the presence of CO₂ at 260 bar. We should point out that the total CO₂ sequestration is calculated from the moles of carbon, C, present in aqueous and solid phases at some specific time, t, after subtracting those at t = 0, then by multiplying by the molecular weight of CO₂ and other unit conversion factors. In addition, CO₂ injection causes a considerable decrease in porosity (compare Figure 2.8 to 2.4), because of enhanced precipitation of the clay mineral smectite-Na. This reduces the amount of CO₂ held in fluid phases, as well as the permeability of the medium. The decreases in porosity and permeability may result in decreasing CO₂ injectivity. Further discussion is given to this matter in Section 5.

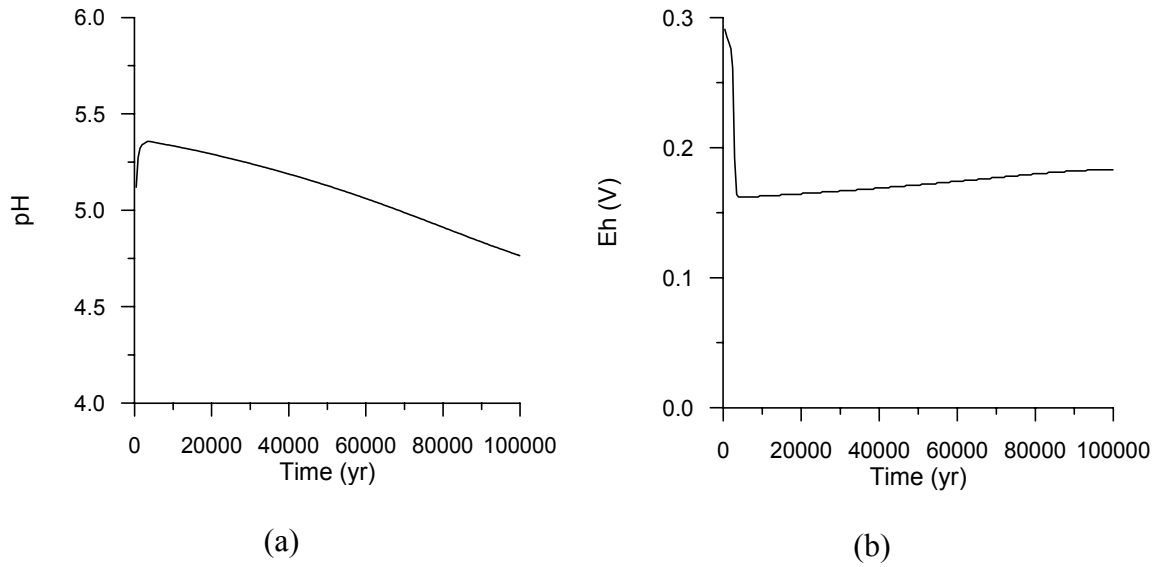


Figure 2.5. Evolution of pH and Eh in glauconitic sandstone (with CO₂ injected at 260 bar).

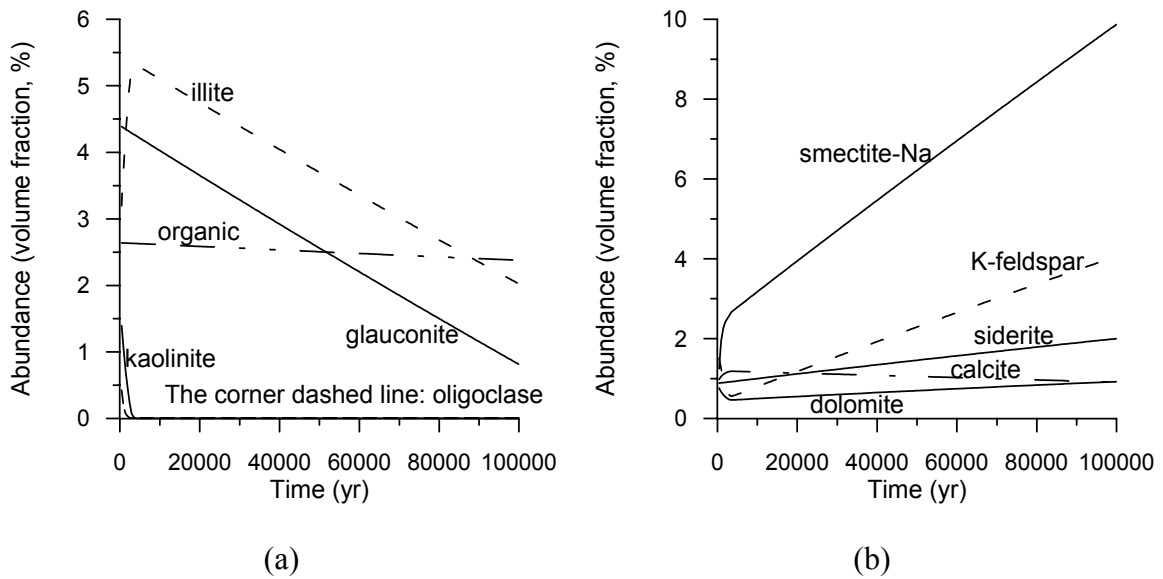


Figure 2.6. Distribution of mineral abundances in glauconitic sandstone (with CO₂ injected at 260 bar).

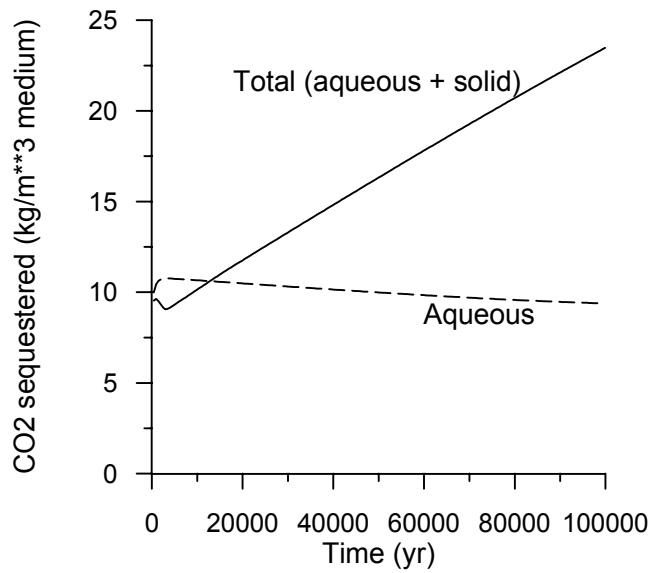


Figure 2.7. Cumulative CO₂ sequestration in glauconitic sandstone (with CO₂ injected at 260 bar).

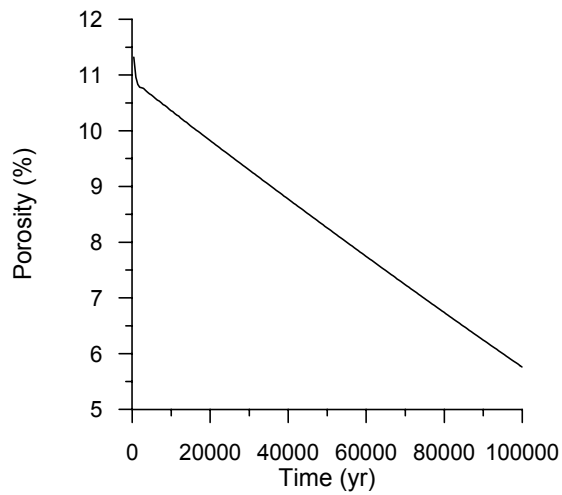


Figure 2.8. Porosity evolution in glauconitic sandstone (with CO₂ injected at 260 bar).

2.3. Sensitivity analysis regarding reaction rates

Estimated mineral dissolution rates cover a wide range of values. The documented values are cited under laboratory conditions of controlled pH and temperature, and fine grain size. Field effective values may be much lower than those reported from laboratory experiments (Nordstrom and Alpers, 1997). The former are complicated by many ill-defined or uncertain factors. However, the important parameter is not the rate constant but the effective rate given by the product of rate constant and reactive surface area (see Eq. C.1 in Appendix C). Great uncertainties also exist as to the appropriate reactive surface area for field simulations. For convenience, we confine our sensitivity analysis only to consideration of reactive surface areas.

The evolution of surface area in natural geologic media is very complex, especially for multi-mineralic systems, and has not yet been quantitatively described. A reactive surface area, calculated from grain size, is often a poor estimate of the hydrologically accessible mineral surface area. The specific reactive surface areas may vary over several orders of magnitude depending on grain size, mineralogy, surface roughness, coatings, weathering, and biological effects (*White and Peterson, 1990*). A sensitivity analysis could give some general understanding of its impact on the overall geochemical behavior of the system. We first performed simulations by scaling the surface areas for all minerals by the same factor, called here “uniform scaling”. Because uniform scaling may be inadequate, we also examined the effect of changing mineral surface areas relative to each another, here called “non-uniform scaling”. All sensitivity simulations are referenced to the previous simulation where glauconitic sandstone is subjected to alteration under a CO₂ injection pressure of 260 bars.

Uniform scaling

We performed two simulations for the uniform scaling by increasing and decreasing the surface areas listed in Table 2.1 by one order of magnitude, respectively. The surface areas for the secondary minerals are changed by the same factors. Sensitivity simulations show that scaling surface areas by the same constant factor is equivalent in scaling the time coordinate and does not lead to different results. Only one figure, that for CO₂ sequestration, is presented to show the effect of uniform scaling, Figure 2.9. By

comparing Figure 2.9 to 2.7, we can see that an increase in the surface areas is equivalent to a corresponding decrease in time scale.

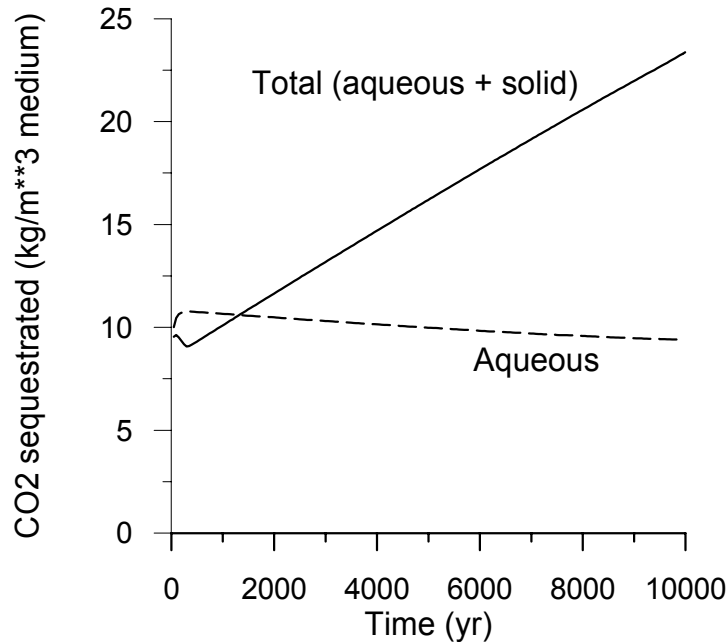


Figure 2.9. Cumulative CO₂ sequestration obtained by increasing the surface areas for all minerals presented in Table 2.1 by one order of magnitude.

Non-uniform scaling

Changes in the specific reactive surface area of any mineral by an increase or a decrease of one order of magnitude, except for glauconite and organic matter do not affect either the dissolution of glauconite and organic matter, or the precipitation of siderite and the amount of CO₂ sequestration. A decrease in the surface area for glauconite relative to other minerals causes a decrease in the dissolution rate of glauconite and illite (compare Figure 2.10a to 2.6a), and thus a decrease in precipitation of siderite and smectite-Na (compare Figure 2.10b to 2.6b). Consequently, the amount of CO₂ sequestration in mineral phases is less than the base case (compare Figure 2.11 to 2.7). An increase in the glauconite surface area has no effect on CO₂ sequestration. Changes in surface area for organic matter have the same patterns as those for glauconite. The dissolution of glauconite and organic matter is redox sensitive. Glauconite dissolution involves a reduction of Fe³⁺ to Fe²⁺. Organic matter dissolution generates CO₂ and CH₄. Therefore, the redox processes drive the entire geochemical system and control

CO₂ sequestration. Further studies on the reduction of glauconite by organic matter may be very important for effective and efficient CO₂ disposal in this type of sediment.

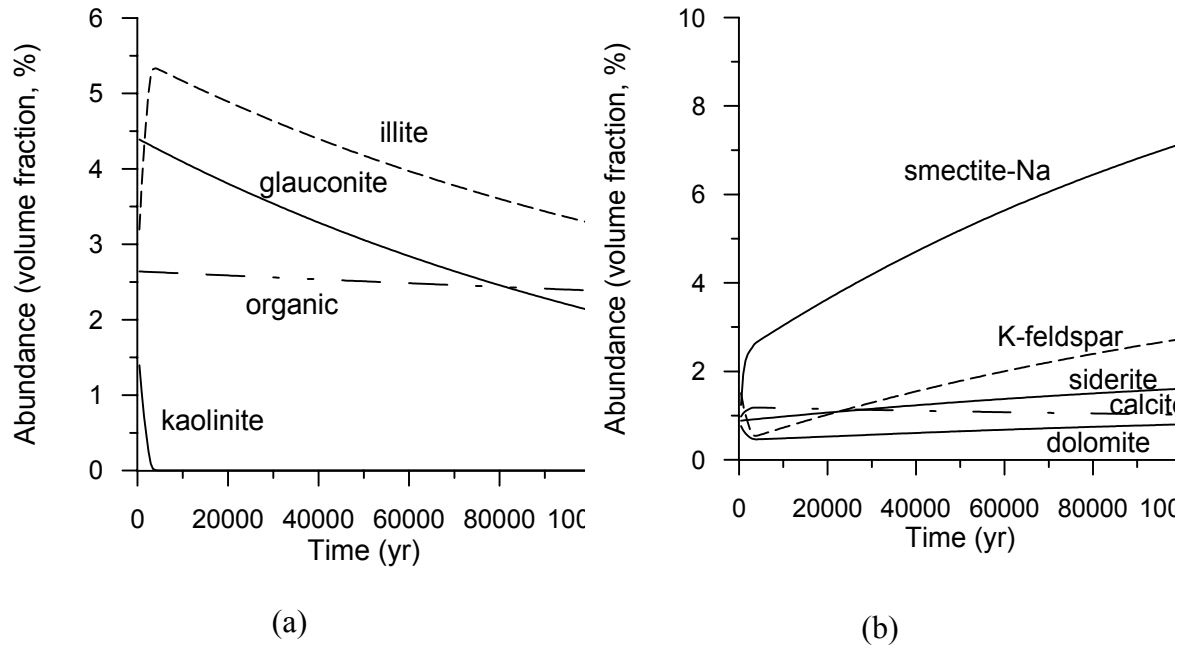


Figure 2.10. Distribution of mineral phases obtained by decreasing glauconite surface area by one order of magnitude and keeping the surface areas for other minerals the same as those presented in Table 2.1.

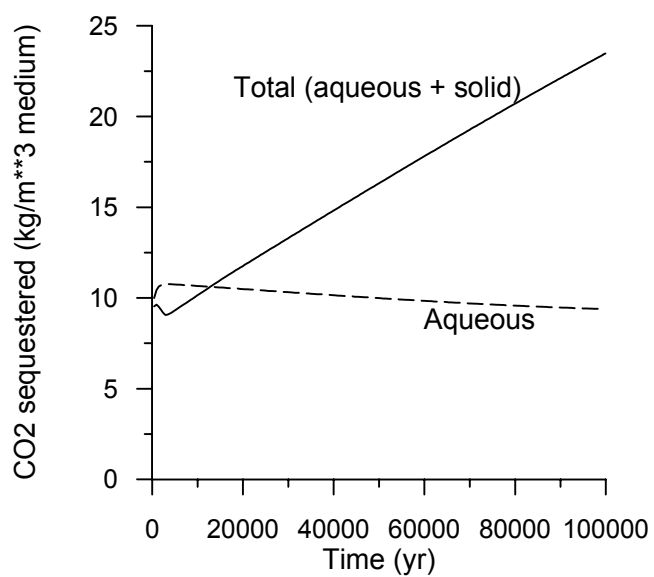


Figure 2.11. Cumulative CO₂ sequestration obtained by decreasing glauconite surface area by one order of magnitude.

3. Gulf Coast Sediments

3.1. Problem Setup

Apps (1996) presented a simulation of the evolution of Gulf Coast sediments as a basis for interpreting the chemical processes relating to the deep injection disposal of hazardous and industrial wastes. Based on data given by the previous investigator, we analyzed the geochemical evolution of Gulf Coast sediments with CO₂ injection. Gulf Coast Mesozoic and Tertiary sediments are characterized by rapid burial and incorporation of significant amounts of organic matter. Maturation of the organic matter into petroleum and natural gas, and its migration into numerous structural traps is a characteristic of these sediments. Therefore, a simulation should incorporate a representation of maturing organic matter. Another feature of relevance is the entrapment of evaporite salt beds during sedimentary accumulation. Over time, the salt has migrated into diapirs, modifying sedimentary accumulation during concurrent sedimentation and subsidence, and generating salt domes, which commonly trap oil and gas accumulations along their flanks. The salt domes are known to partially dissolve into groundwaters, elevating the salinity. Thus a simulation should also include an initial concentration of dissolved sodium chloride.

The initial mineral abundances, based on the rock composition given by Apps (1996), and used in the present simulations are presented in Table 3.1. In treating kinetics of mineral dissolution and precipitation, the rate law and parameters are the same as those used in the previous glauconitic sandstone case. The kinetic parameters employed in the simulation are also given in Table 3.1. Some kinetic parameters were taken directly from the published scientific literature. Others were set to or modified from the known kinetic properties of minerals with similar crystal structures. The treatment of the kinetics of secondary mineral precipitation is also the same as for the previous case.

The initial condition used in the present simulation assumes a pure 1.0 M solution of sodium chloride reacting with the primary minerals listed in Table 3.1 at a temperature of 80°C, a pH of 7, and an Eh of -0.1 V, which is identical to that given by Apps (1996). With increasing time, the water composition will be determined by dissolution of reactant

primary minerals and precipitation of secondary phases. As with the glauconitic sandstone case, the first simulation was of water-rock interaction under natural background conditions without CO₂ injection, in order to provide a basis for comparison. We then introduced a CO₂ injection pressure of 260 bar to the system. The treatment of CO₂ gas phase in the simulation is the same as for the previous case.

The ultimate maturation of organic matter eventually leads to the formation of a carbon-rich residue such as vitrinite or asphaltene. In this study, we assume that this residue is graphite, which we assume precipitates as a result of the dissolution of organic matter. Hence, its kinetic properties are assigned the same values as those of the proxy for organic matter (see Appendix A). The simulation with the addition of possible graphite precipitation is based on the second simulation with CO₂ injection.

Table 3.1. List of initial mineral volume fractions, possible secondary mineral phases, and their kinetic properties. All rate constants are listed for dissolution. The constants for precipitation are increased by one order of magnitude correspondingly. A total surface area of 10 m²/dm³ medium is assumed. The surface area of each primary mineral is calculated from its volume fraction multiplying by the total surface area. Kaolinite, illite and smectite surface areas are increased by two order of magnitude.

Mineral	Chemical composition	Volume (%)	Surface area (m ² /dm ³ medium)	k ₂₅ (moles m ⁻² s ⁻¹)	E _a (KJ/mol)	References
Primary:						
quartz	SiO ₂	46.8	4.68	1.2589x10 ⁻¹⁴	87.50	Tester et al. (1994)
kaolinite	Al ₂ Si ₂ O ₅ (OH) ₄	4.5	0.45x10 ²	1.00x10 ⁻¹³	62.76	Nagy (1995)
calcite	CaCO ₃	15.3	1.53	1.60x10 ⁻⁹	41.87	Svensson and Dreybrodt (1992)
illite	K _{0.6} Mg _{0.25} Al _{1.8} (Al _{0.5} Si _{3.5} O ₁₀)(OH) ₂	4.5	0.45x10 ²	1.00x10 ⁻¹⁴	58.62	Knauss and Wolery (1989)
organic	CH ₂ O	4.5	0.45	1.00x10 ⁻¹³	0.0	assigned based on kaolinite
oligoclase	CaNa ₄ Al ₆ Si ₁₄ O ₄₀	3.6	0.36	1.00x10 ⁻¹²	67.83	set to K-feldspar
pyrite	FeS ₂	4.5	0.45	4.00x10 ⁻¹³	0.0	Ague and Brimhall (1989)
sanidine-high	KAlSi ₃ O ₂	1.8	0.18	1.00x10 ⁻¹²	67.83	Blum and Stillings (1995)
smectite-Ca	Ca _{0.145} Mg _{0.26} Al _{1.77} Si _{3.97} O ₁₀ (OH) ₂	4.5	0.45 x10 ²	1.00x10 ⁻¹⁴	58.62	set to illite
porosity	-----	10				
total	-----	100				
Secondary:						
albite-low	NaAlSi ₃ O ₈	0.0	0.5	1.00x10 ⁻¹²	67.83	Blum and Stillings (1995)
K-feldspar	KAlSi ₃ O ₈	0.0	0.5	1.00x10 ⁻¹²	67.83	Blum and Stillings (1995)
dolomite	CaMg(CO ₃) ₂	0.0	0.5	0.60x10 ⁻⁹	41.8	assigned based on calcite
siderite	FeCO ₃	0.0	0.5	0.60x10 ⁻⁹	41.8	assigned based on calcite
smectite-Na	Na _{0.290} Mg _{0.26} Al _{1.77} Si _{3.97} O ₁₀ (OH) ₂	0.0	0.5x10 ²	1.00x10 ⁻¹⁴	67.83	set to illite

3.2. Results

Background without CO₂ injection

The evolution of pH and Eh is presented in Figure 3.1. A pH of 9.15 is maintained until 75000 years when oligoclase dissolves completely (Figure 3.3a). After that, a step decrease of pH to 5.4 occurs. The values of Eh respond similarly, but in a reciprocal manner. The partial pressures of some gaseous species are presented in Figure 3.2. In this simulation, the calculation method for the partial pressure is the same as that for the previous case. CH₄ is generated throughout the simulation time. CO₂ only appears after the pH decreases to 5.4. From Figure 3.2a, we can see that CO₂ partial pressure is much lower than that of CH₄. We should note that solubility of CO₂ is over one order of magnitude larger than that of CH₄. So the amount of CO₂ in the aqueous phase is comparable to that of CH₄. H₂ is generated at lower values of Eh (Figure 3.2b), whereas H₂S appears at higher values of Eh. The step changes in the gas pressures are consistent with the changes in pH and Eh, which are caused by disappearance of oligoclase. The very large CH₄ partial pressures in Figure 3.2a are a reflection of the closed batch system modeled here. In reality, the geochemical system is “open”, i.e., CH₄ (as well as CO₂) will not all remain in place, but can be transported in flowing groundwater as well as a free gas phase. These phenomena will be addressed in the future reactive geochemical transport modeling.

We now turn our attention to the distribution of mineral phases. Sanidine-high is destroyed very rapidly (Figure 3.3a). Illite and smectite-Ca are stable when oligoclase is present. After complete oligoclase dissolution, illite dissolves, and smectite precipitates and then dissolves. Organic matter dissolution occurs at a constant rate as in the previous case. Pyrite is stable in this environment. Calcite, kaolinite, and K-feldspar precipitation occurs throughout the simulation. Albite-low precipitates until the disappearance of oligoclase, then starts to dissolve. Dolomite and siderite are not formed in this simulation. Porosity (Figure 3.4) at first increases, and then decreases. The change in direction of porosity evolution coincides with that of the disappearance of oligoclase.

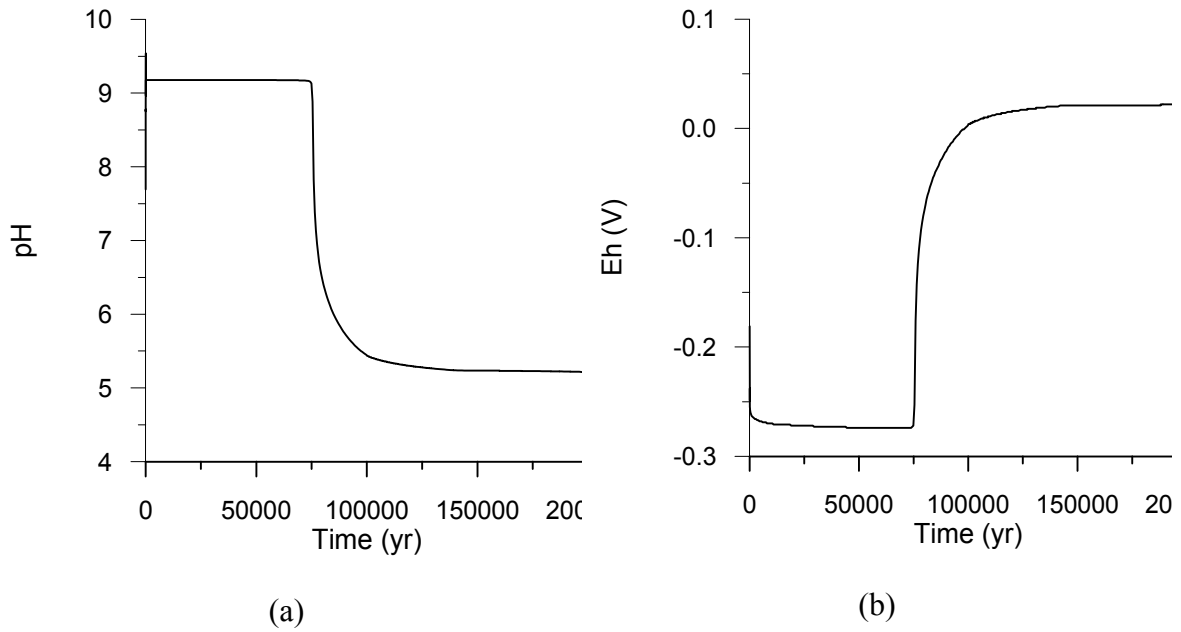


Figure 3.1. Evolution of pH and Eh obtained with interaction of groundwater with Gulf Coast sediments (background case).

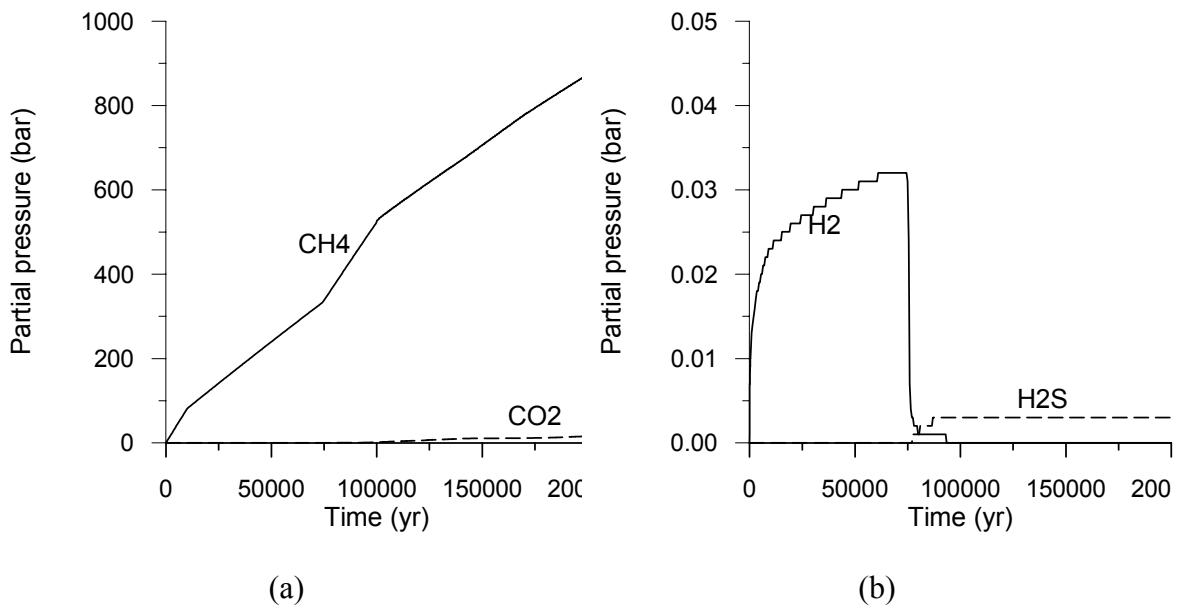


Figure 3.2. Distribution of gaseous partial pressures obtained with interaction of groundwater with Gulf Coast sediments (background case).

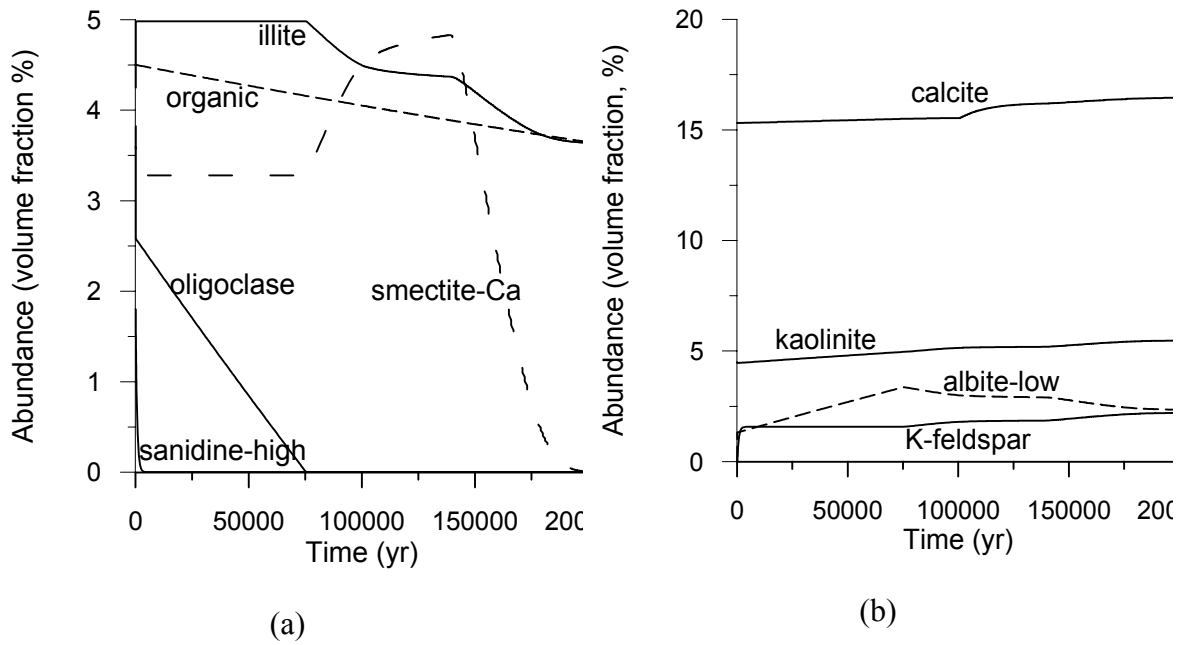


Figure 3.3. Distribution of mineral phases obtained with interaction of groundwater with Gulf Coast sediments (background case).

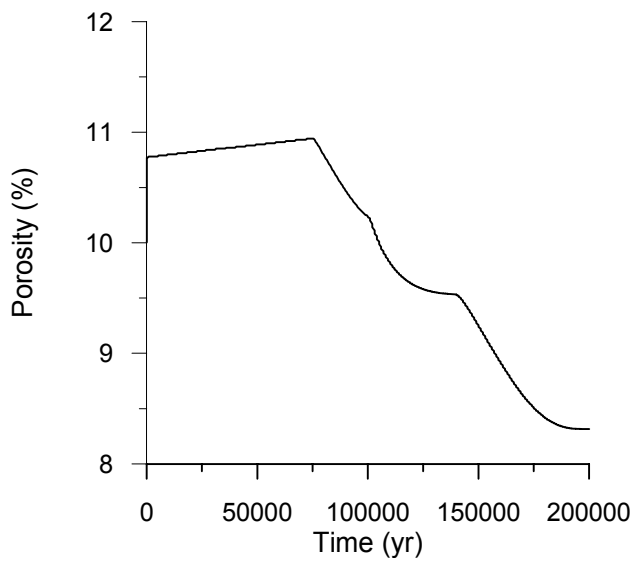
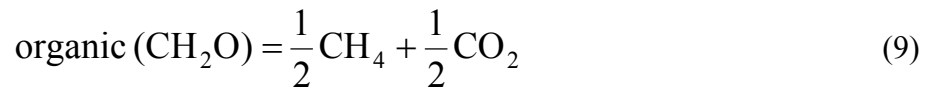


Figure 3.4. Porosity evolution obtained with interaction of groundwater with Gulf Coast sediments (background case).

With CO₂ injection

The pH and Eh (Figure 3.5), obtained with a CO₂ injection pressure of 260 bar, are strongly buffered by the gas pressure (compare Figure 3.5 to 3.1). By comparing with the background simulation, only CH₄ is generated but much less is produced (compare Figure 3.6 to 3.2a). Furthermore, H₂ and H₂S are not present, because this environment is more oxidizing (i.e., a higher Eh). The distribution of mineral phases is presented in Figure 3.7. Oligoclase, sanidine-high, and smectite-Ca are destroyed very rapidly (after 450 years). After disappearance of these minerals, the system reaches a relatively stable condition except for the dissolution of organic matter, which proceeds at a constant rate. Initially, calcite precipitates, and sequesters a maximum of about 7 kg per m³ medium in the solid phase (Figure 3.8). Later, the amount of sequestered CO₂ decreases. As mentioned in the glauconitic sandstone case, the CO₂ sequestration shown in Figure 3.8 is calculated by the change in moles of carbon inventory multiplied by the molecular weight and some unit conversion factors. The decrease in CO₂ sequestration means that some CO₂ leaves the system. This is because calcite precipitation stops, but organic matter dissolution still proceeds at the same rate. The dissolution of 1 mole of organic matter produces one half mole CH₄ and one half mole CO₂, thus:



In this simulation, a constant CO₂ gas pressure of 260 bar is imposed from $t = 0$. The gas phase is treated as an exterior boundary in the modeling. This treatment of the gas phase may overestimate somewhat the decrease in CO₂ sequestration. The simulated porosity evolution is presented in Figure 3.9

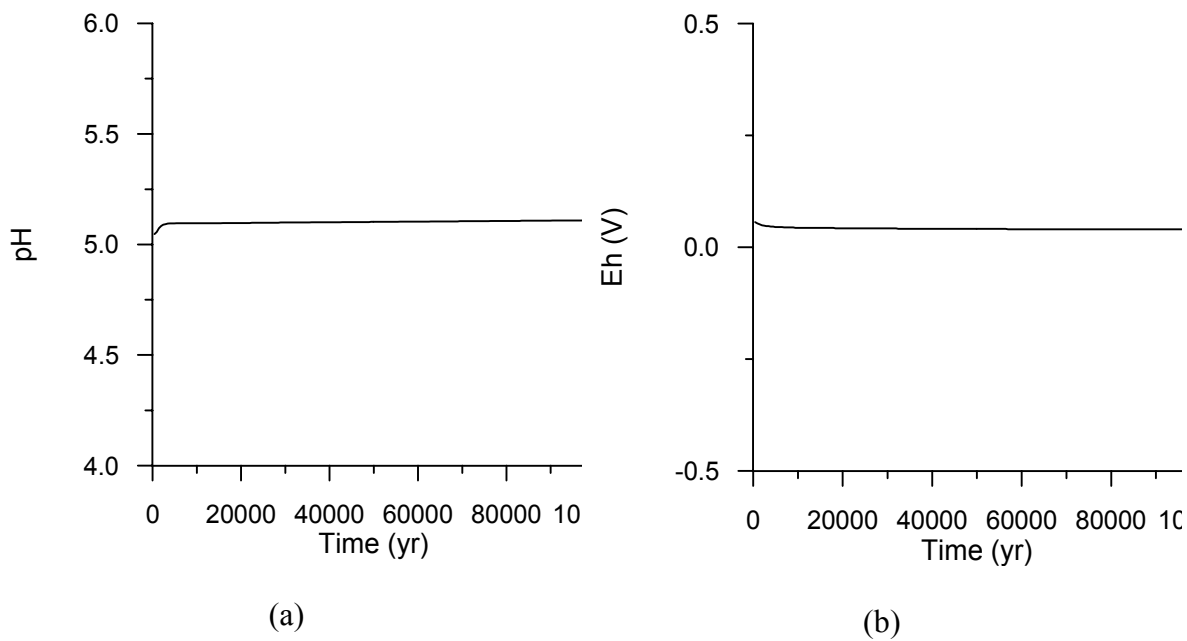


Figure 3.5. Evolution of pH and Eh obtained during the interaction of groundwater with Gulf Coast sediments (with CO₂ injected at 260 bar).

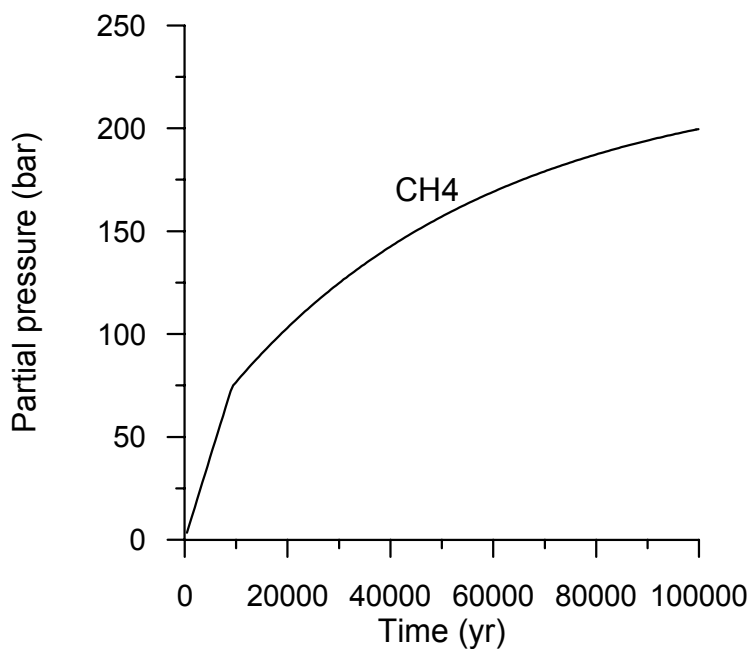


Figure 3.6. Distribution of gaseous partial pressure obtained during the interaction of groundwater with Gulf Coast sediments (with CO₂ injected at 260 bar).

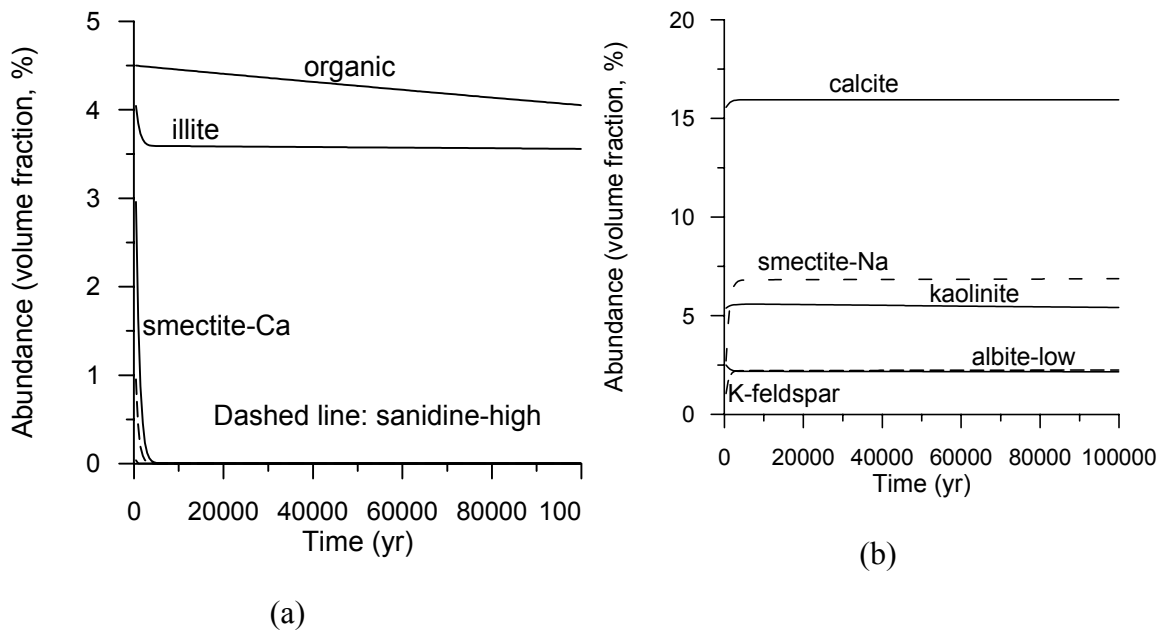


Figure 3.7. Distribution of mineral phases obtained during the interaction of groundwater with Gulf Coast sediments (with CO₂ injected at 260 bar).

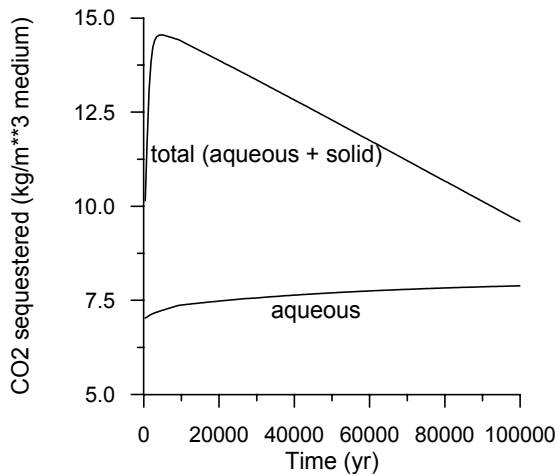


Figure 3.8. Cumulative CO₂ sequestration obtained during the interaction of groundwater with Gulf Coast sediments (with CO₂ injected at 260 bar).

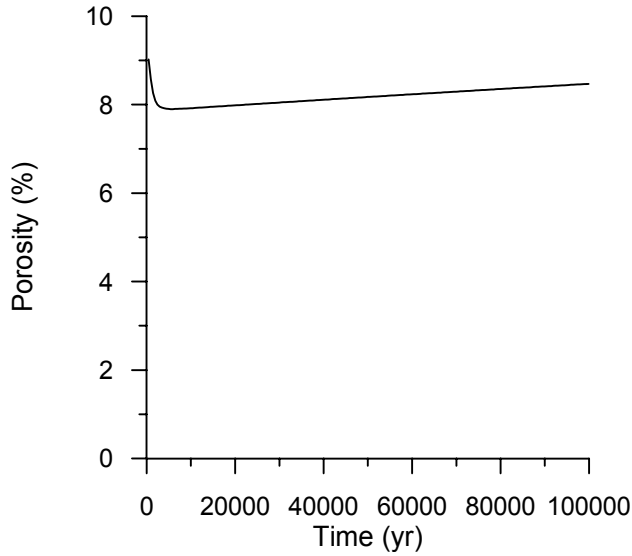


Figure 3.9. Porosity evolution obtained during the interaction of groundwater with Gulf Coast sediments (with CO₂ injected at 260 bar).

Considering graphite precipitation

The pH and Eh obtained by considering graphite precipitation are similar to those without considering it (Figure 3.5). However, in the latter case, CH₄ is not generated. Graphite precipitation occurs (Figure 3.10a). Unlike the previous simulation without considering graphite precipitation, calcite precipitates continuously (Figure 3.10b). The resulting mineral assemblage is similar. Continuous calcite precipitation results in steadily increasing CO₂ sequestration with time (Figure 3.11), whereas in the previous simulation, the CO₂ sequestration is not stable (Figure 3.8). A consequence is that porosity (Figure 3.12) decreases with time as CO₂ is immobilized in the mineral phase (calcite).

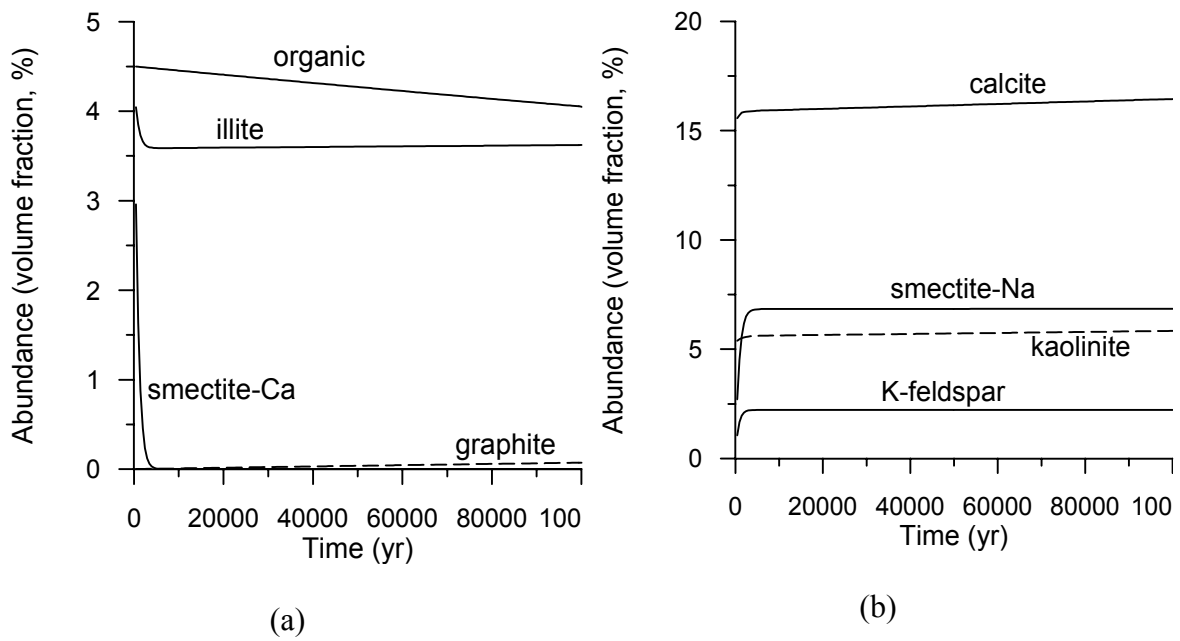


Figure 3.10. Distribution of mineral phases obtained with CO₂ injection considering graphite precipitation for Gulf Coast sediments.

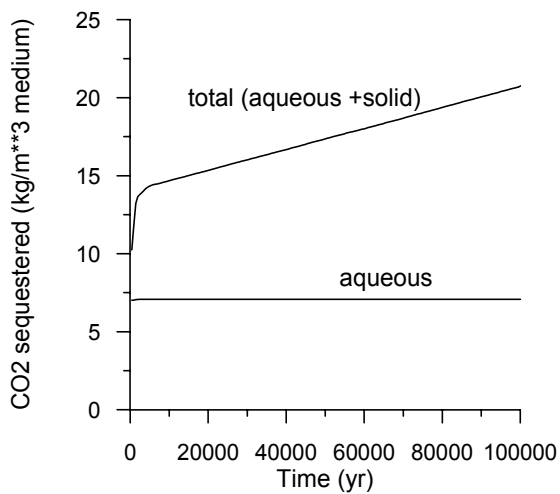


Figure 3.11. Cumulative CO₂ sequestration obtained with CO₂ injection considering graphite precipitation for Gulf Coast sediments.

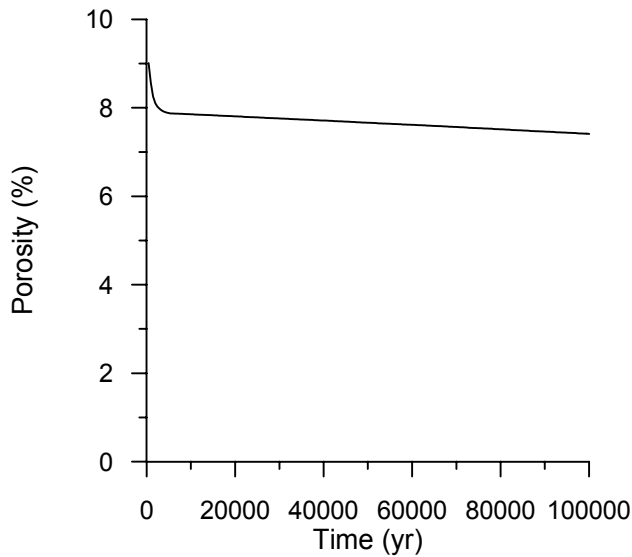


Figure 3.12. Porosity evolution obtained with CO₂ injection considering graphite precipitation for Gulf Coast sediments.

4. Dunite

4.1. Problem Setup

Olivine, the predominant mineral of depleted mantle rock, commonly referred to as dunite, has one of the largest CO₂ sequestration capabilities of all minerals (see Appendix B). Olivine is a binary solid solution of two pure end-member components, forsterite (Mg₂SiO₄) and fayalite (Fe₂SiO₄). The volume ratio of these end member components in typical olivine is about 9:1. The initial mineral abundances used in the simulations are presented in Table 4.1. The porosity of dunite is commonly small. We used an initial porosity of 0.05. The possible secondary mineral phases under natural conditions and CO₂ injection are also listed in Table 4.1. The treatment of kinetics for mineral dissolution and precipitation, and kinetic rate law used are the same as those of the previous two sedimentary rock cases.

The initial condition used is a dilute solution reacting with the primary minerals listed in Table 4.1 with a temperature of 80°C, a pH of 7, a Eh of -0.1 V. With increasing time, the water composition will be determined by dissolution of reactant primary minerals and precipitation of secondary phases. In conformity with the previous two

sedimentary rock cases, we started with a simulation of water-rock interaction under natural background conditions. We then introduced a CO₂ injection pressure of 260 bar to the system. The treatment of CO₂ gas phase in the simulation is the same as in the previous cases.

Table 4.1. List of initial mineral volume fractions, possible secondary mineral phases, and their kinetic properties. All rate constants are listed for dissolution. The constants for precipitation are increased by one order of magnitude correspondingly. A total surface area of 10 m²/dm³ medium is assumed. The surface area of each primary mineral is calculated from its volume fraction multiplying by the total surface area. The kinetic data for magnesite and siderite are modified from those of calcite (Table 3.1). The kinetic data for other minerals are set equal to those of kaolinite (Table 3.1).

Mineral	Chemical composition	Volume (%)	Surface area (m ² /dm ³ medium)	k ₂₅ (moles m ⁻² s ⁻¹)	E _a (KJ/mol)
Primary:					
forsterite	Mg ₂ SiO ₄	85.5	8.55	1.00x10 ⁻¹³	62.76
fayalite	Fe ₂ SiO ₄	9.5	0.95	1.00x10 ⁻¹³	62.76
porosity	-----	5.0			
total	-----	100			
Secondary:					
magnetite	Fe ₃ O ₄	0.0	0.5	1.00x10 ⁻¹³	62.76
magnesite	MgCO ₃	0.0	0.5	0.60x10 ⁻⁹	41.87
siderite	FeCO ₃	0.0	0.5	0.60x10 ⁻⁹	41.87
talc	Mg ₃ Si ₄ O ₁₀ (OH) ₂	0.0	0.5	1.00x10 ⁻¹³	62.76
chrysotile	Mg ₃ Si ₂ O ₅ (OH) ₄	0.0	0.5	1.00x10 ⁻¹³	62.76
greenalite	Fe ₃ Si ₂ O ₅ (OH) ₄	0.0	0.5	1.00x10 ⁻¹³	62.76
amorphous silica	SiO ₂	0.0	0.5	1.00x10 ⁻¹³	62.76
sepiolite	Mg ₄ Si ₆ O ₁₅ (OH) ₂ (H ₂ O) ₆	0.0	0.5	1.00x10 ⁻¹³	62.76
iron	Fe	0.0	0.5	1.00x10 ⁻¹³	62.76
graphite	C	0.0	0.5	1.00x10 ⁻¹³	62.76

4.2. Results

Background without CO₂ injection

pH and Eh remain stable at values of 10.7 and -0.52 V throughout the simulation time. The system is therefore strongly reducing. H₂ generation occurs continuously. Forsterite and fayalite also dissolve continuously. Iron, magnetite, and chrysotile precipitation occurs. As a result, the porosity decreases to 0.5% after 15000 years.

With CO₂ injection

After a CO₂ gas pressure of 260 bar is imposed, the pH decreases to 4.8, and Eh increases to 0.1 V. In this more oxidizing environment, H₂ is not generated and pure iron (Fe) is not precipitated. The distribution of mineral phases is presented in Figure 4.1. Forsterite and fayalite dissolution occurs at constant rates. As a result, magnesite and siderite precipitate due to the dissolution of the two primary reactant minerals and the CO₂ supply from injection. At the same time, talc and amorphous silica precipitation occurs. Chrysotile, greenalite, sepiolite, and graphite are not formed. CO₂ sequestration proceeds at a constant rate because of the constant precipitation of magnesite and siderite. After 1000 years, about 100 kg CO₂ is immobilized in one m³ medium (Figure 4.2). Theoretically, a much higher amount (more than 1000 kg) of CO₂ can be sequestered because forsterite and fayalite are still abundant after this time. However, the porosity (Figure 4.3) has decreased to 0.6%. There is little free space to accommodate water and CO₂. The rock alteration and CO₂ sequestration processes would terminate when the porosity had declined to a negligible value.

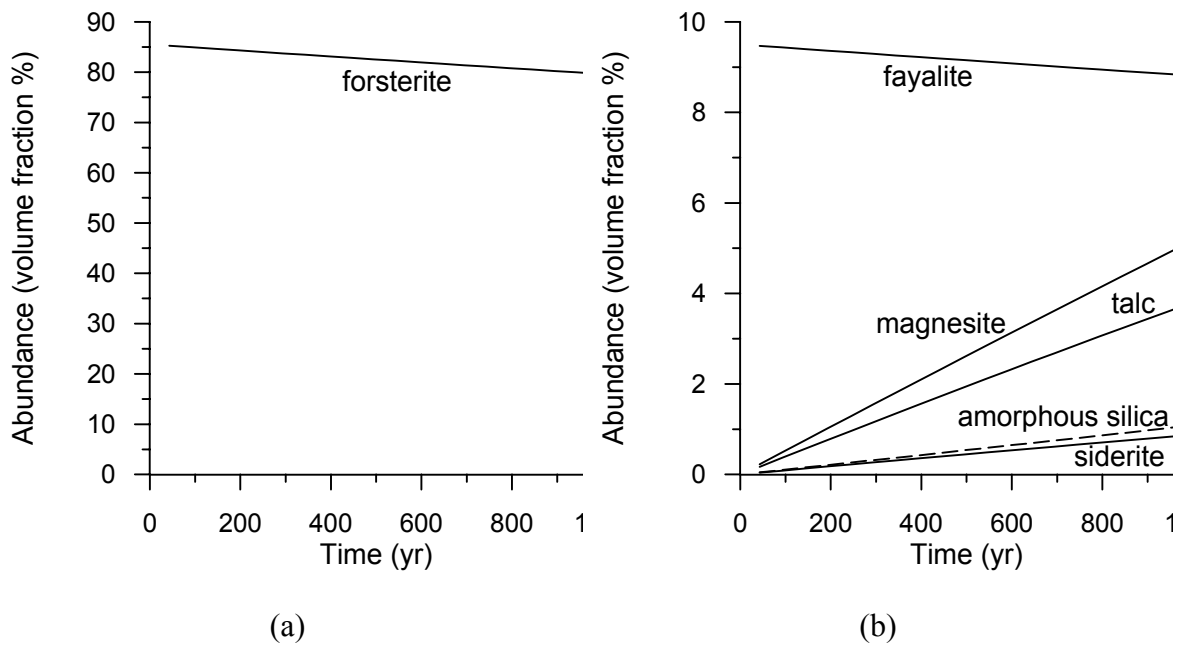


Figure 4.1. Distribution of mineral phases obtained with CO₂ injection for the olivine rock.

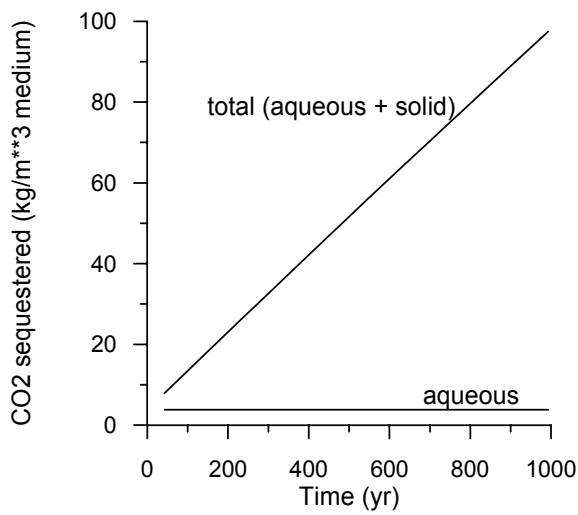


Figure 4.2. Cumulative CO₂ sequestration for the olivine rock.

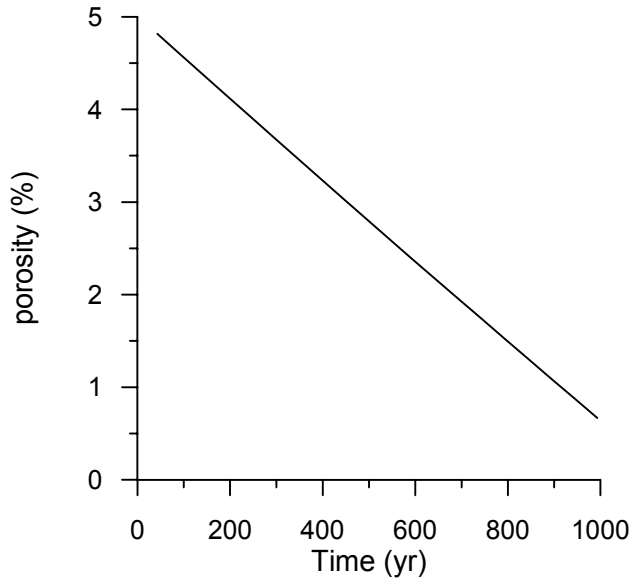


Figure 4.3. Porosity evolution obtained with CO₂ injection for the olivine rock.

5. Discussion

In the foregoing simulations, three naturally occurring rock assemblages have been subjected to alteration under various constraints under natural diagenetic conditions and in the presence of a supercritical CO₂ fluid. The immediate impression gained from examination of all simulations in the absence of supercritical CO₂ is that they reveal reassuring similarities to field observations of corresponding diagenetic processes. However, a detailed comparison of the simulations with field observations will require additional effort. The volume of literature describing the diagenetic processes of rocks corresponding to those employed in the simulations is substantial, and will require careful scrutiny. Furthermore, earlier investigators did not have access to powerful simulators now readily available, and were therefore not in a position to ask the pertinent questions demanded by model requirements. Such investigators are also likely to have missed subtleties critical to model substantiation or rejection. Such deficiencies are likely to make detailed analysis and refinement of the geochemical models a painstaking process, which is beyond the scope of this preliminary analysis.

Several features of the simulations serve to highlight the need for a more critical evaluation both of the kinetic parameters required of the models, and of the role that organic matter and its decomposition play in the control of redox processes in the system. It is evident from the limited number of model simulations that the rate of decomposition of organic matter can ultimately affect the rate of CO₂ sequestration by secondary carbonates, especially siderite. The fact that the dissolution or decomposition of certain species can control the overall rate of sequestration was not immediately apparent at the beginning of this investigation, and the implications are still not fully understood. It is also clear that the complexities associated with quantitative prediction of heterogeneous processes implicit in diagenesis need further elucidation and clarification if more realistic and quantifiable modeling is to be conducted successfully. For while the current investigation clearly indicates that the thermodynamic description of the current models demonstrate a semi-quantitative measure of realism, the quantitative kinetic aspects are at best intelligent guesses. Further detailed analysis, again beyond the scope of this preliminary study, is clearly mandated.

The simulations involving glauconitic sandstone and Gulf Coast aquifer arenite are satisfactory, although certain features of these simulations require refinement. In both rock types, chlorite has been omitted as a reactant or potential product mineral. Generally, chlorite is a relatively minor mineral in sandstones, but it is commonly present, and sometimes quite abundant in associated shales. Long term exposure of such shales to supercritical CO₂ under hydrous conditions could lead to their alteration to silica, kaolinite, magnesite and siderite. The relative stability of chlorite with respect to silica polymorphs, kaolinite, and Mg and Fe(II) carbonates at reservoir temperatures and pressures should be explored further.

The carbonate mineral, ankerite, has also been omitted from simulations involving glauconitic and Gulf Coast sandstones, because no thermodynamic data have been published, and therefore its solubility product is unknown. Ankerite is a relatively common cementitious diagenetic alteration product in Gulf Coast sediments, and would probably precipitate as an alteration product in the presence of high CO₂ partial pressures. However, ankerite is of very variable composition, and further investigation is required

not only to define the compositional ranges expected in sedimentary environments, but also to estimate its thermodynamic properties.

Another issue meriting further comment is the use of the component CH_2O as proxy for organic matter. Its decomposition, or solubilization with consequent formation of carbon dioxide, graphite or methane, depending on the oxidation state of the system at the time, is at best an extremely crude representation of the petroleum maturation process. Furthermore, petroleum maturation usually occurs at temperatures higher than those specified for the simulations in this study. A more realistic representation of the role that organic matter plays in modifying or controlling the oxidation state of the system at temperatures lower than those characteristic of non-condensable gas or petroleum maturation is called for. Because of the apparently high activation energy involved in the maturation of organic matter in sediments, it is possible that bacterial processes play a catalytic role, even in deep aquifers. The role of bacteria in the decomposition of organic matter in sediments has long been recognized, but the impact of high ambient CO_2 partial pressures on bacterial activity has not been explored. Further investigation of the preceding issues is certainly merited if more realistic simulations are to be conducted in the future.

The simulation of olivine hydrolysis and the resultant formation of such secondary minerals as native iron, magnetite and chrysotile is generally consistent with the serpentinization of ultra-mafic rocks. Furthermore, the development of extreme reducing conditions, manifested by the evolution of hydrogen gas, is also consistent with field observations (Apps and Van de Kamp, 1993). However, ultra-mafic rocks usually contain other minor components, which are also affected by the extremely reducing conditions induced by the hydrolysis of ferrous iron. Because these components have been omitted, the application of natural analogues for validation would necessarily require more detailed simulations. Despite the inherent limitations of this test case, the simulation results are encouraging and fully justify further development.

The alteration of ultramafic rocks under sub-critical hydrous conditions, while being simultaneously subjected to elevated CO_2 pressures, is a less likely natural scenario, although possible in active mafic volcanic plate margins. An important feature of the alteration process is the substantial positive volume change of the solid phases

upon alteration, due not only to the formation of secondary hydrated phase, but also to the formation of magnesite and siderite. Volume expansion upon serpentinization of ultramafics has long been recognized in the literature, and implicit in this process is the elimination of residual porosity. The almost complete serpentinization of ultramafic rocks in ophiolitic assemblages suggests that the elimination of porosity is not of itself sufficient to prevent total serpentinization. The heavily fractured nature of serpentinites in the field, and multiple generations of sealed fractures, suggests that active tectonism may facilitate the process. Such conditions, however, would almost certainly disqualify any potential carbon dioxide reservoir for safety reasons.

5.2. Capacity for CO₂ sequestration by minerals

For the glauconitic sandstone aquifer, our simulation suggests that a small amount of CO₂ is sequestered through precipitation of calcite (CaCO₃) and dolomite (CaMg(CO₃)₂). A significant amount of CO₂ is trapped by precipitation of siderite (FeCO₃). This is because the solubilities of calcite and dolomite are much larger than siderite. The total amount of CO₂ trapped in mineral phases could reach about 15 kg per m³ of medium (Figure 2.7), which is greater than that dissolved in the aqueous phase (about 10 kg per m³ of medium). The precipitation of siderite, either as a discrete carbonate or as a solid solution in more abundant Ca-Mg carbonates, or as ankerite ((Mg,Ca,Fe(II))CO₃), is conditioned by the redox state of the system. However, even relatively low partial pressures of H₂S would favor the fixation of Fe²⁺ as pyrite. This may considerably decrease CO₂ sequestration in mineral phases. For the Gulf Coast sediments, the only CO₂ trapping mineral to appear is calcite (Figure 3.10). CO₂ trapped in calcite could reach 7 kg per m³ of medium. If graphite precipitation is also considered, this amount is about two times greater than that trapped in the aqueous phase (7 kg per m³ of medium). The precipitation of calcite and mineral trapping of CO₂ strongly depend on graphite precipitation kinetics. The slower the formation of graphite, the slower is calcite precipitation. As an extreme case without considering graphite precipitation, calcite precipitation occurs only after a short period of time (Figure 3.7b). Even though organic matter continues to dissolve (Figure 3.7a), CO₂ generated from organic matter leaves the system, and the CO₂ sequestration processes stops (Figure 3.8). It should be

pointed out that the treatment of constant CO₂ gas pressure may overestimate somewhat this effect. Dunite would have the largest capacity for CO₂ sequestration. One m³ of medium could sequester as much as 100 kg CO₂ as secondary carbonates (Figure 4.2). However, this type of rock is not found in significant amount in the earth's crust. From our analysis, we note that mineral trapping of CO₂ varies considerably with rock type. For the two sedimentary rocks presented, glauconitic sandstone has a greater CO₂ mineral trapping capability under a suitable redox environment than Gulf Coast sediments. The trapping capabilities also depend on other factors such as gas pressure, temperature, porosity and mineral composition. For the glauconitic sandstone case, the sequestration capacity is proportional to abundances of both glauconite and organic matter. In all three cases presented, mineral-trapping capacity is comparable with, and can be larger than that of solubility trapping.

Korbol and Kaddour (1995) conducted a simulation study to evaluate CO₂ distribution for the Sleipner Vest project in the Norwegian sector of the North Sea, using a two-phase flow simulator, but without considering geochemical processes. Their results indicated that up to 18% of the CO₂ injected was dissolved in the formation water. Thus, the largest CO₂ trapping mechanism is that of hydrodynamic trapping. Even though mineral trapping is not the largest mechanism, sequestration is essentially permanent.

5.3. Changes in porosity

All three examples demonstrate that rock alteration after CO₂ injection results in decreased porosity (Figures 2.8, 3.12, and 4.3). This is because (1) CO₂ mass is added to the solid matrix, and (2) some altered mineral products have lower densities, such as clay minerals. A small decrease in porosity can result in a significant decrease in permeability. The decrease could reduce the CO₂ injectivity. The change in porosity is therefore a very important issue for CO₂ injection into deep geologic formations. Ross et al (1982) observed a decreasing injectivity during CO₂ injection for enhanced oil recovery. (Sayegh et al., 1990, and Bowker and Shuler, 1991) conducted a lab experiment on the injection of supercritical CO₂ into core samples of sandstone, and showed that core permeability remained the same or decreased. We should note that the laboratory experimental times were short compared to those of our model simulations. Therefore, permeability change

due to mineral alteration and the secondary precipitation of carbonates is unlikely to be observed.

5.4. Time required for sequestration

The time needed to sequester CO₂ in mineral phases is uncertain, because mineral kinetic properties and reactive surface areas are not well constrained. Sensitivity simulations show that scaling surface areas by the same constant factor is equivalent in scaling the time coordinate and does not lead to different results. An increase in the surface areas is equivalent to a decrease in time scale. Similarly, the converse is true. Changes in the specific reactive surface area for a redox sensitive mineral such as glauconite or organic matter significantly affect mineral alteration, and consequently the amount of CO₂ sequestration. Further studies on the uncertainty of kinetic properties, especially for redox sensitive minerals, should be addressed by laboratory and field experiments, and numerical simulations. The reaction time is a relative concept, and is affected by the fluid transport time scale. The reaction may be fast enough to form effective CO₂ mineral traps given a long residence time of a packet of fluid in a deep aquifer. The difference of the two time scales may help ensure that CO₂ mineral trapping would be complete before any packet of fluid reaches the surface. Modeling of geochemical processes under dynamic fluid flow conditions will be performed in the future. The reactive geochemical transport modeling reported here may give some understanding of the time scale.

5.5. Limitations of geochemical modeling

Because of the chemical complexity of injection induced water-CO₂-rock interaction processes, an extensive theoretical framework is required to support the modeling of such systems. This framework is rarely if ever fully incorporated in geochemical models, nor are the algorithms used in geochemical codes always sufficient to meet the challenges involved. The range of problems for CO₂ in subsurface environments is far more extensive than any code presently accommodates. Because of numerous uncertainties and approximations, numerical simulation results may not completely match field observations of mineral alteration. For example, the kinetics of

heterogeneous reactions are scale and history-dependent, and cannot be reliably quantified. Reactive surface areas are notoriously uncertain and subject to poorly quantifiable phenomena such as the armoring of mineral phases by others. Furthermore, there is a lack of sufficiently detailed geochemical data at field sites. Because of these factors, modeling cannot give a complete quantitative prediction of geochemical evolution of CO₂ injection. Instead, modeling is a good and unique tool for analyzing and evaluating long-term CO₂ sequestration and geochemical performance. The “numerical experiments” give a detailed understanding of the dynamic evolution of the geochemical systems. A critical evaluation of modeling results can provide useful insight into sequestration mechanisms and controlling geochemical conditions and parameters.

5.6. Effects of physical processes on geochemistry

For large-scale injection of CO₂ into aquifers, geochemical processes are strongly affected by physical processes such as multiphase fluid flow, solute transport, and changes in effective stress. Fluid pressures will rise as CO₂ displaces aquifer water in which it partly dissolves. The dissolution of primary and precipitation of secondary minerals changes formation porosity and permeability, and then fluid flow pattern. The continuous injection of CO₂ will lead to increased formation pressures over large areas, of the order of 100 km² or more, which will modify the local mechanical stress field, causing deformation of the aquifer. All processes involving coupled hydrologic, mechanical and chemical effects influence the feasibility of CO₂ injection and storage in deep aquifers. No comprehensive coupled approaches have yet been used to analyze aquifer CO₂ disposal systems. Uncoupled batch geochemical modeling, flow simulations, and rock stress analyses are inadequate in describing the complex subsurface physical and chemical interactions expected to occur. A systematic process-based understanding of the coupled physical and chemical phenomena should be addressed in the future.

6. Conclusions

Three host rock types have been evaluated for long-term CO₂ disposal in deep aquifers using a geochemical modeling tool. Major conclusions that can be drawn are as follows:

- (1) The simulated mineral assemblages are generally consistent with field observations. However, all simulations contain omissions or simplifications mandated by current limitations concerning knowledge of the thermodynamic properties of participating minerals and the kinetics of phase transformations. A critical review of the literature describing the diagenetic processes observed in rocks corresponding to those selected for modeling in this report is needed to identify unrecognized deficiencies in the current simulations and allow progressive refinement of future simulations.
- (2) CO₂ sequestration by mineral phases varies considerably with rock type. Gulf Coast sediments have the smallest capacity (13 kg per m³ of medium). The capacity of a glauconitic sandstone aquifer (15 kg per m³ of medium) is only incrementally larger than that of Gulf Coast sediments. Dunite has the largest sequestration capacity (100 kg per m³ of medium). However, this rock type is rarely found in crustal rocks, and its fortuitous occurrence in a structural trap is unlikely. The trapping capacity depends on many factors such as porosity and mineral composition. For the glauconitic sandstone case, the capacity is proportional to the abundances of both glauconite and organic matter. The formation of CO₂-trapping mineral phases is case-dependent. For the glauconitic sandstone case, most CO₂ is trapped as siderite, with minor calcite and dolomite. For the Gulf Coast case, the only trapping mineral is calcite. For the olivine rock (dunite) case, the trapping minerals are magnesite and siderite. In all three cases presented, the mineral trapping capacity can be comparable with, and is larger than, that of solubility trapping (7-10 kg per m³ of medium).
- (3) The time frame for CO₂ sequestration is a function of reaction kinetics. Sensitivity simulations show that scaling surface areas by the same constant factor is equivalent in scaling the time coordinate and otherwise does not lead to different results. The surface area changes lead to reciprocal changes in the

time scale. Specific changes in the reactive surface area for redox sensitive minerals such as glauconite or organic matter significantly affect mineral alteration and the extent of CO₂ sequestration.

- (4) Carbon dioxide induced rock mineral alteration and the addition of CO₂ mass as secondary carbonates to the solid matrix results in decreased porosity. This in turn adversely affects permeability and fluid flow in the aquifer. Porosity decreases could reduce the CO₂ injectivity. Porosity degradation might be a more important issue than CO₂ sequestration itself. Decreasing injectivity has been observed in the field during CO₂ injection for enhanced oil recovery.

The range of problems concerning the interaction of water-CO₂-rock is very broad. The present simulation results are specific to the conditions and parameters considered. Care should be taken when extrapolating the results and conclusions for other sites. The “numerical experiments” give a detailed understanding of the dynamic evolution of a particular geochemical system. A critical evaluation of modeling results can provide useful insight into sequestration mechanisms and controlling geochemical conditions and parameters.

Appendix A. Estimation of Thermodynamic Properties of Minerals required for Reaction Progress Simulations

Appendix B. Availability of Rock-forming Chemical Components that Can Sequester Carbon Dioxide as Solid Carbonates.

Sequestration or fixation of carbon dioxide in subsurface rock formations depends on the availability and quantities of metal oxide components that can react with carbon dioxide to form solid carbonates with low solubility. Table B.1 gives a list of the elements of these oxide components, and their absolute abundance in the earth's crust. Only a limited suite of rock forming chemical components possesses the required properties. In order of abundance, they are FeO, CaO, MgO, MnO, SrO and BaO. At elevated temperatures, these components combine with silica, and sometimes in combination with alumina, to form minerals that compose common igneous and metamorphic rocks. When these rocks weather under conditions at or near the earth's surface, the primary rock forming minerals decompose at various rates, and react with carbon dioxide in the atmosphere to produce secondary carbonates. Upon exposure to the atmosphere, FeO and MnO components react with oxygen to form trivalent or tetravalent oxides respectively, which do not react to form carbonates. Both FeO and MnO are therefore able to sequester carbon dioxide only under low temperature reducing conditions, such as might occur in buried sedimentary rocks containing reducing agents such as organic residues. The alkali earth metal oxides, CaO, SrO and BaO can also form low-solubility sulfates, the relative stability of the carbonate or sulfate being determined by the potentials of CO₂ or SO₃ in a given environment.

Table B.1. Concentration of carbonate forming elements in the earth's crust

Element	Concentration, ppm
Fe	50,000
Ca	36,300
Mg	20,900
Mn	1,000
Sr	450
Ba	400
Ni	80
Zn	65
Cu	45
Co	23
Pb	15

Source: Mason (1958)

The abundance and availability of sequestering oxide components depends on the nature of the rock and the rock forming minerals containing those components. These minerals can be conveniently divided into classes with similar crystal structures:

Framework Silicates

- **Plagioclase**
- Barium feldspars
- Sodalite
- Cancrinite
- Scapolite
- Zeolite Group

Ortho and ring silicates

- **Olivine Group**
- Garnet group
- Epidote group

- Melilite group
- Calcium
- Borosilicates
- Various calcium-containing metamorphic minerals (stauolite, vesuvianite, sphene, chloritoid, lawsonite, pumpellyite, cordierite)

Chain Silicates

- **Pyroxene group**
- **Amphibole group**
- Wollastonite
- Pectolite
- Rhodonite
- Pyrox-manganite

Sheet silicates

- **Mica Group**
- **Septechlorite group**
- **Chlorite group**
- **Clay Minerals**
- **Talc**
- Stilpnomelate
- **Serpentine**
- Apophyllite
- Prehnite

The above classification has been abstracted from Deer et al. (1963a, b, c, d, and e). Other classifications of the rock-forming minerals may differ in detail. The bold-faced minerals or mineral groups are most abundant. The abundance of a given mineral or

mineral group depends both on the bulk composition of the rock and the nature of its formation. Thus olivines characteristically are major constituents of rocks forming depleted mantle, such as the ultramafic rock, dunite. Serpentine is a major constituent of serpentinite, which is an alteration product of ultramafic rock such as dunite. Both rock types are exposed at the earth's surface primarily in active tectonic regions, but are relatively uncommon elsewhere.

Table B.2 lists the major mineral series within each group and specifies the maximum quantity of carbon dioxide that could be sequestered by each mineral. The potential values are calculated by assuming complete alteration of the primary minerals.

Table B.2. Carbon dioxide sequestration potential of major rock forming minerals

Mineral Name	Mineral Formula	Potential CO ₂ Fixed, kg/m ³ mineral
Plagioclase (anorthite)	Ca[Al ₂ Si ₂ O ₈]	436.4
Ba-Feldspar-Celsian	Ba[Al ₂ Si ₂ O ₈]	398.2
Sodalite Group-Hauyne	(Ca) ₄ [Al ₆ Si ₆ O ₂₄](SO ₄)	383.8
Cancrinite	(Ca) _{1.5} [Al ₆ Si ₆ O ₂₄](CO ₃) ₁₋₅ .1.5H ₂ O	132.5
Scapolite (meionite)	(Ca) ₄ [Al ₆ Si ₆ O ₂₄](CO ₃)	387.3
Zeolites-Heulandite	Ca ₄ Na[Al ₉ Si ₂₇ O ₇₂].24H ₂ O	138.4
-Laumontite	Ca[Al ₂ Si ₄ O ₁₂].6H ₂ O	208.1
-Scolecite	Ca[Al ₂ Si ₃ O ₁₀].3H ₂ O	254.9
-Chabazite	(Ca,Na ₂)[Al ₂ Si ₄ O ₁₂].6H ₂ O	176.5
-Thomsonite	NaCa ₂ [Al ₅ Si ₅ O ₂₀].6H ₂ O	258.7
Olivine (forsterite-fayalite)	Mg ₂ SiO ₄ - Fe ₂ SiO ₄	2014.7-1896.3
Garnet Group-Almandine	Fe(II) ₃ Al ₂ Si ₃ O ₁₂	1144.7
-Andradite	Ca ₃ Fe(III) ₂ Si ₃ O ₁₂	1002.3
-Grossular	Ca ₃ Al ₂ Si ₃ O ₁₂	1053.1
-Pyrope	Mg ₃ Al ₂ Si ₃ O ₁₂	1164.9
-	Ca ₃ Al ₂ Si ₂ O ₈ (OH) ₄	974.8
Hydrogrossular		
Epidote Group-Epidote	Ca ₂ Fe(III)Al ₂ O.OH[Si ₂ O ₇][SiO ₄]	628.8
Melilite Group-Gehlenite	Ca ₂ [Al ₂ SiO ₇]	972.4
-Akermanite	Mg ₂ [AlSi ₂ O ₇]	1423.0
Ca Borosilicates-Datolite	CaB[SiO ₄](OH)	825.6
Staurolite	(Fe(II),Mg) ₂ (Al,Fe(III)) ₉ O ₆ [SiO ₄] ₂ (O,OH) ₄	394.7
Vesuvianite	Ca ₁₀ (Fe(II),Mg) ₂ (Al,Fe(III))Al ₃ O ₂ [SiO ₄] ₂ (OH) ₄	1167.0
Chloritoid	(Mg,Fe) ₂ Al ₄ [Si ₂ O ₇][SiO ₄] ₈ (OH) ₄	629.8
Lawsonite	CaAl ₂ (OH) ₂ [Si ₂ O ₇]H ₂ O	422.7
Pumpellyite	Ca ₄ (Mg,Fe(II))(Al,Fe(III)) ₅ (OH) ₃ [Si ₂ O ₇] ₂ [SiO ₄] ₂ .2 H ₂ O	735.6
Cordierite	Al ₃ (Mg,Fe(II)) ₂ [Si ₅ O ₁₈]	749.4
Pyroxene group-Enstatite	(Mg,Fe) ₂ Si ₂ O ₆	1404.2
-Diopside-Hedenbergite	CaMgSi ₂ O ₆ -Ca(Mg,Fe(II))Si ₂ O ₆	1334.3-1290.3
Augite	(Ca,Mg,Fe(II),Al) ₂ (Si,Al) ₂ O ₆	1306.3
Pigeonite	(Mg,Fe(II),Ca)(Mg,Fe(II)),Fe(III),Al)Si ₂ O ₆	1345.4
Amphibole group-Anthophyllite-Cummingtonite	(Mg,Fe(II),Fe(III)) ₅₋₇ Al ₀₋₂ [Si ₆₋₈ Al ₂₋₀ O ₂₂](OH) ₂	1169.5-1041.8
Common Hornblende	Ca ₂ Na ₀₋₁ (Mg,Fe(II)) ₃₋₅ (Al,Fe(III)) ₂₋₀ [Si ₆₋₈ Al ₂₋₀ O ₂₂](O,OH) ₂	1000.4
-Calcium Amphiboles-tremolite	Ca ₂ Na ₀₋₁ (Mg,Fe(II)) ₃₋₅ (Al,Fe(III)) ₂₋₀ [Si ₆₋₈ Al ₂₋₀ O ₂₂](O,OH) ₂	1119.3
-Alkali	Na ₂₋₃ Ca ₀₋₁ (Mg,Fe(II)) ₅₋₃ (Al,Fe(III)) ₀₋₂ Si ₇₋₈ Al ₁₋	496.3

Amphiboles-glaucophane	${}_0\text{O}_{22}](\text{O},\text{OH})_2$	
Wollastonite	CaSiO_3	1097.1
Pectolite	$\text{Ca}_2\text{NaH}[\text{SiO}_3]_3$	761.1
Mica group-Glauconite	$(\text{K},\text{Na},\text{Ca})_{1.2-2.0}(\text{Fe(III)},\text{Al},\text{Fe(II)},\text{Mg})_{4.0}[\text{Si}_{7-7.6}\text{Al}_{1-0.4}\text{O}_{20}](\text{OH})_4.n\text{H}_2\text{O}$	61.97
Mica group-Phlogopite	$\text{K}_2(\text{Mg},\text{Fe(II)})_6[\text{Si}_6\text{Al}_2\text{O}_{20}](\text{OH})_4$	881.8
Mica group-Biotite	$\text{K}_2(\text{Mg},\text{Fe(II)})_{6-4}(\text{Fe(III)},\text{Al})_{0-2}[\text{Si}_{6-5}\text{Al}_{2-3}\text{O}_{20}](\text{OH})_{4-2}$	671.0
Mica group-Margarite	$\text{Ca}_2\text{Al}_4[\text{Si}_4\text{Al}_4\text{O}_{20}](\text{OH})_4$	328.6
Septechlorite Group		
-Serpentine	$\text{Mg}_6\text{Si}_4\text{O}_{10}(\text{OH})_8$	1232.7
-Greenalite	$\text{Fe(II)}_6\text{Si}_4\text{O}_{10}(\text{OH})_8$	1140.1
Chlorite Group	$(\text{Mg},\text{Al},\text{Fe(II)})_{12}[(\text{Si},\text{Al})_8\text{O}_{20}](\text{OH})_{16}$	923.4
Clay Minerals-illite	$\text{K}_{1-1.5}(\text{Fe(III)},\text{Al},\text{Fe(II)},\text{Mg})_{4.0}[\text{Si}_{7-6.5}\text{Al}_{1-1.5}\text{O}_{20}](\text{OH})_4$	78.42
Clay Minerals-smectite	$(1/2\text{Ca},\text{Na})_{0.7}(\text{Al},\text{Mg},\text{Fe})_4(\text{Si},\text{Al})_8\text{O}_{20}(\text{OH})_4.n\text{H}_2\text{O}$	161.2
Talc	$\text{Mg}_6[\text{Si}_8\text{O}_{20}](\text{OH})_4$	1061.2
Stilpnomelane	$(\text{K},\text{Na},\text{Ca})_{0-1.4}(\text{Fe(III)}, \text{Fe(II)}), \text{Mg}, \text{Al}, \text{Mn})_{5.9-8.2}[\text{Si}_8\text{O}_{20}](\text{OH})_4(\text{O}, \text{OH}, \text{H}_2\text{O})_{3.6-8.5}$	266.5
Prehnite	$\text{Ca}_2\text{Al}[\text{AlSi}_3\text{O}_{10}](\text{OH})_2$	626.9

Notes

- (1) Many of the above minerals are solid solutions whose compositions vary depending on the bulk composition and prior history of the host rock
 - (2) Some of the mineral groups are represented only by typical examples rather than being comprehensive, such as the zeolites, which contain many different structures.
 - (3) Minerals containing an essential component with low crustal abundance have been omitted.
 - (4) Minor non-essential substitutive components in solid solutions have been omitted
- ?5? Zeolite cell parameters used in the calculation of CO₂ sequestration potential, are from Gottardi and Galli (1985). All other cell parameters have been taken from Deer et al. (1963a, b, c, d, and e).

In assuming the value of minerals in the CO₂ sequestration process, several factors must be considered:

- The nature of the host rock, i.e. whether igneous, metamorphic, or sedimentary
- The origin of the mineral, whether primary, authigenic, detrital or secondary
- The effective reactivity of the mineral in the host rock. This is a function of the permeability and porosity of the host rock, the mineral specific surface area, the decomposition mechanism and rate, and whether or not reaction products interfere with continued decomposition.
- The mass fraction of reactive minerals in a given host rock.

- The accessibility of water in permitting mineral decomposition and reaction of the dissolved constituents with CO₂.

In general, in most plutonic igneous and metamorphic rock masses, the rock matrix permeability and porosity are very low. The permeability is determined primarily by the presence, type and orientation of fractures. Furthermore, the rock forming minerals are commonly quite coarsely crystalline and therefore slow to react, because the mineral specific surface area is low. Finally, if supercritical CO₂ were to be injected into the fractures, the availability of water would be limited to that in the pores of the rock matrix, which, in the course of time would be consumed by hydrated reaction by-products, thereby inhibiting mineral dissolution/precipitation and shutting down the sequestration process. Finally, the irregular shape and mass of such rock limits the extent to which injected CO₂ would be confined. In most cases, confinement is achieved by transecting faults sealed by fault gouge or metamorphic aureoles whose fractures are sealed by deuteritic minerals. Such confining structures are notoriously difficult either to characterize or identify in the field. Thus igneous and metamorphic rock bodies are normally unpromising hosts for subsurface disposal or sequestration of CO₂, despite their apparently favorable rating on purely chemical grounds.

Most extrusive igneous rocks are subject to similar limitations for the disposal of CO₂, particularly if they happen to be lavas. The most extensive are flood basalts, found covering large areas of the earth's surface in certain parts of the world. Basalts are commonly heavily fractured, and also possess vesicular porosity. Both microcrystalline groundmass and residual glass contain significant CaO, MgO and FeO. Therefore they could be favorable candidate host rocks for CO₂ sequestration. However, the generally low permeability and porosity of the matrix would suggest that reaction rates would be very low. If the basalt flows are buried and overlain by impermeable sedimentary cap rocks, they could be potential repositories of supercritical CO₂, particularly if tectonic deformation were to create structural traps. Mafic vitroclastic ash-fall tuffs (hyaloclastites) would be an even more favorable host rock for CO₂ sequestration, because their porosity and permeability would be very high. But their uncommon

occurrence and even less likely structural containment make such deposits unlikely candidates for CO₂ sequestration. Furthermore, their high reactivity causes hyaloclastites to decompose rapidly to secondary smectites, whose permeability is quite low.

The most likely candidates for CO₂ storage and sequestration are sedimentary aquifer rocks with relatively high porosity and permeability, such as sandstones. Their capacity for sequestration depends on the presence of detrital minerals containing reactive carbonate forming components. The major mineral forming any sandstone is, of course, quartz, which is essentially inert, the remaining detrital minerals being the weathering products of precursor igneous, metamorphic or sedimentary rocks. Minerals comprising precursor crystalline igneous and metamorphic rocks display varying resistance to weathering. Micas, some pyroxenes and amphiboles, plagioclase and potash feldspars, and some minerals characteristic of metamorphic terrains, such as the amphiboles and staurolite typically weather sufficiently slowly that they are incorporated in sedimentary formations before complete decomposition. Other minerals, such as olivine, weather relatively rapidly, and are rarely incorporated in sedimentary rocks. Those products of chemical weathering of primary rock-forming minerals that would react and sequester CO₂ are primarily phyllosilicates, such as clays, illite and smectite, septechlorites, chlorites and talc. These minerals can be incorporated as a minor detrital constituent of sandstones, or they are present as included lenses or confining shale layers.

Some authigenic minerals, such as glauconite, bertierine and authigenic iron sulfides could also play a role in CO₂ sequestration, but such minerals form under relatively restricted conditions, and while not uncommon, should be considered only on a case by case basis.

Appendix C. Main features of TOUGHREACT model

Present simulations are carried out using the non-isothermal reactive geochemical transport code TOUGHREACT (Xu and Pruess, 1998 and 2000). This model was developed by introducing reactive chemistry into the framework of the existing multi-phase fluid and heat flow code TOUGH2 (Pruess, 1991). The flow and transport in geologic media are based on space discretization by means of integral finite differences (Narasimhan and Witherspoon, 1976). An implicit time-weighting scheme is used for flow, transport, and geochemical reaction. TOUGHREACT uses a sequential iteration approach, which solves the transport and the reaction equations separately. TOUGHREACT can also be used for batch geochemical modeling. As only geochemical modeling features are used in the present simulations, so we only present TOUGHREACT features on geochemistry.

The system of chemical reaction equations is solved by a Newton-Raphson iterative method similar to that of Parkhurst (1980), Reed (1982), and Wolery (1992). Full details on numerical methods are given in Xu and Pruess (1998). The model can accommodate any number of chemical species present in liquid, gas and solid phases. Aqueous chemical complexation and gas (CO_2) dissolution/exsolution are considered under the local equilibrium assumption. Mineral dissolution/precipitation can proceed either subject to local equilibrium or kinetic conditions. Thermodynamic and kinetic data are functions of temperature. The formulation of chemical equilibrium is similar to that by Parkhurst (1980), Reed (1982), Yeh and Tripathi (1991), Wolery (1992), and Steefel and Lasaga (1994). The activity of aqueous species is equal to the product of the activity coefficient and molar concentration. Aqueous species activity coefficients with the exception of $\text{CO}_2(\text{aq})$ are calculated from the extended Debye-Hückel equation (Helgeson and Kirkham, 1974). The calculations of $\text{CO}_2(\text{aq})$ activity coefficient and $\text{CO}_2(\text{g})$ fugacity coefficient are presented in Appendix D. Activities of pure mineral phases and H_2O are assumed to be one. Mass conservation in the closed chemical system is written in terms of basis species. The species distribution must be governed by the total concentrations of

the components. The oxygen approach is used for formulating redox reactions, which is based on attributing the oxidizing potential to the dissolved oxygen (Nordstrom and Muñoz, 1986; Wolery, 1992).

For kinetically-controlled mineral dissolution and precipitation, a general form of rate law (Lasaga, 1984; and Steefel and Lasaga, 1994) is used

$$r_m = A_m k_m \left[1 - \left(\frac{Q_m}{K_m} \right)^\mu \right]^n \quad (C.1)$$

where m is mineral index, r_m is the dissolution/precipitation rate (positive values indicate dissolution, and negative values precipitation), A_m is the specific reactive surface area per kg H_2O , k_m is the rate constant (moles per unit mineral surface area and unit time) which is temperature dependent, K_m is the equilibrium constant for the mineral-water reaction written for the destruction of one mole of mineral m , Q_m is ion activity product, The parameters μ and n are two positive numbers normally determined by experiment, and are usually, but not always, taken equal to unity. The temperature dependence of the reaction rate constant can be expressed reasonably well via an Arrhenius equation (Lasaga, 1984; and Steefel and Lasaga, 1994). Since many rate constants are reported at 25 °C, it is convenient to approximate rate constant dependency as a function of temperature, thus

$$k = k_{25} \exp \left[\frac{-E_a}{R} \left(\frac{1}{T} - \frac{1}{298.15} \right) \right] \quad (C.2)$$

where E_a is the activation energy, k_{25} is the rate constant at 25 °C, R is gas constant, and T is absolute temperature.

Appendix D. Treatment of CO₂ in the calculations

Interaction of gaseous and aqueous CO₂ species, CO₂(g) = CO₂(aq), is assumed at equilibrium. According to the mass-action law, we have

$$K\Gamma P = \gamma C \quad (D.1)$$

where K is the equilibrium constant, Γ is the gaseous CO₂ fugacity coefficient, P is the partial pressure (bar), γ is the aqueous CO₂ activity coefficient, and C is the aqueous concentration (mol/kg H₂O).

Equilibrium constant K at different temperatures can be derived from the following expression:

$$\log K = b_1 \ln T + b_2 + b_3 T + \frac{b_4}{T} + \frac{b_5}{T^2} \quad (D.2)$$

where the values of the coefficients b_1 , b_2 , b_3 , b_4 and b_5 are obtained from the logK values at 0, 25, 60, 100, 150, 200, 250, and 300°C. Based on logK values at these temperatures given in EQ3/6 geochemical database (Wolery, 1992), we obtained the following values of the coefficients: $b_1 = 65.48$, $b_2 = -425.5$, $b_3 = -0.05301$, $b_4 = 24010$, $b_5 = -1.22 \times 10^6$. We did not consider pressure dependence of K values. However, in the EQ3/6 database the pressure for log K values below 100°C is 1 bar and for those above 100°C is water saturated pressure.

At low pressures (in the range of atmospheric pressure), the gaseous species is assumed to behave as an ideal mixture, and the fugacity coefficient is assumed equal to unity. At higher temperatures and pressures, such as CO₂ deep aquifer disposal (as applies to the conditions presented here) and boiling conditions in hydrothermal systems, the assumption of ideal gas and ideal mixing behavior is not valid, and the fugacity coefficients should be corrected according to temperatures and pressures of the study system (Spycher and Reed, 1988). For the present H₂O-CO₂ mixture conditions, we

assume that H₂O and CO₂ are real gases, but ideal mix. According to Spycher and Reed (1988), the fugacity coefficients can be calculated from

$$\ln \Gamma = \left(\frac{a}{T^2} + \frac{b}{T} + c \right) P + \left(\frac{d}{T^2} + \frac{e}{T} + f \right) \frac{P^2}{2} \quad (D.3)$$

where P is the total gas pressure (vapor and CO₂), T is absolute temperature, and a, b, c, d, e, and f are constants fitted from experimental data. For P-T ranges, 50-350 °C, up to 500 bars, the fitted constants have the following values: a = -1430.87, b = 3.598, c = -2.27376×10⁻³, d = 3.47644, e = -1.04247×10⁻², and f = 8.46271×10⁻⁶. Examples of equilibrium calculations between aqueous and gas phases show that ideal mixing of real gases is an adequate approximation in the above-mentioned P-T ranges (Spycher and Reed, 1988).

For low ionic strength solution, CO₂(aq) activity coefficient γ can be assumed equal to one. For high ionic strength sodium chloride solution, γ should be corrected (salting out effect). Here we use an activity coefficient expression of Drummond (1981) for the neutral CO₂(aq) species:

$$\ln \gamma = \left(C + FT + \frac{G}{T} \right) I - (E + HT) \left(\frac{I}{I+1} \right) \quad (D.4)$$

where T is the absolute temperature, I is ionic strength (or sodium chloride molality), C, F, G, E, and H are constants (C=-1.0312, F=0.0012806, G=255.9, E=0.4445, and H=-0.001606). This expression was previously used in geochemical modeling codes EQ3/6 (Wolery, 1992). The ionic strength I is defined by

$$I = \frac{1}{2} \sum_i c_i z_i^2 \quad (D.5)$$

where the summation is over all aqueous species, and c_i and z_i are concentration (mol/kg H₂O) and electrical charge of species i.

Acknowledgement. We are grateful to Ardyth Simmons and Nicolas Spycher for a review of the manuscript and suggestions for improvement. This work was supported by the Assistant Secretary for Sciences, Office of Basic Energy Sciences, of the U.S. Department of Energy, under Contract No. DE-AC03-76SF00098 with Lawrence Berkeley National Laboratory.

References

- Ague, J. J., and Brimhall, G. H., 1989, Geochemical modeling of steady state and chemical reaction during supergene enrichment of porphyry copper deposits, *Economic Geology*, v. 84, p. 506-528.
- Apps, J. A., and Van de Kamp, P. C., 1993. Energy gases of abiogenic origin in the earth's crust, In the future of energy gases, United States Geological Survey professional paper 1570, p. 81-132.
- Apps, J. A., 1996, An approach to modeling of the chemistry of waste fluid disposal in deep saline aquifers, In Apps, J. A., and Tsang, C. F. (eds.), Deep injection disposal of hazardous and industrial waste: Scientific and Engineering Aspects, p. 465-488, Academic Press, San Diego, California.
- Bachu, S., Gunter, W. D., and Perkins, E.H., 1994, Aquifer disposal of CO₂: hydrodynamic and mineral trapping, *Energy Convers. Mgmt.*, V. 35, p. 269-279.
- Blum, A. E., and Stillings, L. L., 1995, Feldspar dissolution kinetics, Chapter 7 of chemical weathering rates of silicate minerals, White, A.F., and Brantley, S. L. (eds.), *Mineral Society of America*, v. 31, p. 291-351, Washington D. C.
- Bowker, K. A., and Shuler, P. J., 1991, Carbon dioxide injection and resultant alteration of the Weber sandstone, Rangely Field, Colorado, Bulletin of The American Association of Petroleum Geologists, V. 75, No. 9, p. 1489-1499.
- Deer, W. A., Howie, R. A., and Zussman, J., 1963a, Rock-Forming Minerals, v. 1, Ortho and Ring Silicates, John Wiley and Sons, Inc., 333 p.
- Deer, W. A., Howie, R. A., and Zussman, J., 1963b. Rock-Forming Minerals, v. 2, Chain Silicates, John Wiley and Sons, Inc., 379 p.

- Deer, W. A., Howie, R. A., and Zussman, J., 1963c, Rock-Forming Minerals, v. 3, Sheet Silicates, John Wiley and Sons, Inc., 270 p.
- Deer, W. A., Howie, R. A., and Zussman, J., 1963d, Rock-Forming Minerals, v. 4, Framework Silicates, John Wiley and Sons, Inc., 435 p.
- Deer, W. A., Howie, R. A., and Zussman, J., 1963e, Rock-Forming Minerals, v. 5, Non Silicates, John Wiley and Sons, Inc., 371 p.
- Drummond, J. M., Jr., 1981, Boiling and mixing of hydrothermal fluids: Chemical effects on mineral precipitation, Ph.D. thesis, The Pennsylvania State University, University Park, Pennsylvania.
- Gottardi, G., and Galli, E., 1985, Natural zeolites, Minerals and Rocks, v. 18, Springer-Verlag, Berlin, 409 p.
- Gunter W. D., Perkins, E. H., and McCann, T. J., 1993, Aquifer disposal of CO₂-rich gases: Reaction design for added capacity. *Energy Convers. Mgmt.*, V. 34, p. 941-948.
- Gunter W. D., Bachu, S., Law, D. H. S., Marwaha, V., Drysdale, D. L., MacDonald, D. E., and McCann, T. J., 1996, Technical and economic feasibility of CO₂ disposal in aquifers within the Alberta Sedimentary Basin, Canada, *Energy Convers. Mgmt.* V. 37, p. 1135-1142.
- Gunter W. D., Wiwchar, B., and Perkins, E. H., 1997, Aquifer disposal of CO₂-rich greenhouse gases: extension of the time scale of experiment for CO₂-sequestering reactions by geochemical modeling, *Mineral. and Petrol.*, V. 59, p. 121-140.
- Helgeson, H. C., and Kirkham, D. H., 1974, Theoretical prediction of the thermodynamic behaviour of aqueous electrolytes at high pressures and temperatures: II. Debye-Hückel parameters for activity coefficients and relative partial molal properties: *American Journal of Science*, v. 274, p. 1199-1261.
- Hitchon, B. (ed.), 1996, *Aquifer Disposal of Carbon Dioxide*, Geoscience Publishing, Ltd., Sherwood Park, Alberta, Canada.
- Holloway, S., and Savage, D., 1993, The potential for aquifer disposal of carbon dioxide in the UK. *Energy Convers. Mgmt.*, V. 34, p. 925-932.
- Holloway, S., 1997, An overview of the underground disposal of carbon dioxide, *Energy Convers. Mgmt.*, v. 38, p. 193-198.

- Johnson, J. W., Oelkers, E. H., and Helgeson, H. C., 1992, SUPCRT92: A software package for calculating the standard molal thermodynamic properties of minerals, gases, aqueous species, and reactions from 1 to 5000 bars and 0 to 1000 degrees C, *Computers and Geosciences*, v. 18, p. 899–947.
- Knauss, K. G., and Wolery, T. J., 1989, Muscovite dissolution kinetics as a function of pH and time at 70°C.” *Geochimica et Cosmochimica Acta*, V. 53, p. 1493–1501.
- Korbol, R. and Kaddour, A., 1995, Sleipner vest CO₂ disposal - injection of removed CO₂ into the Utsira Formation, *Energy Convers. Mgmt.*, V. 36, No. 6-9, p. 509-512.
- Lasaga, A. C., 1981, Dynamic treatment of geochemical cycles: Global kinetics. In: Kinetics of geochemical processes, *Reviews in Mineralogy*, V. 8, eds. Lasaga, A.C., and Kirkpatrick, R.J., p. 69-110, Mineralogical Society of America, Washington D.C.
- Lasaga, A. C., 1984, Chemical kinetics of water-rock interactions, *Journal of Geophysical Research*, v. 89, p. 4009-4025.
- Law, D. H. S., and Bachu, S., 1996, Hydrogeological and numerical analysis of CO₂ disposal in deep aquifers in the Alberta Sedimentary Basin, *Energy Convers. Mgmt.*, V. 37, No. 6-8, p. 1167 - 1174.
- Lohuis, J. A. O., 1993, Carbon dioxide disposal and sustainable development in The Netherlands, *Energy Convers. Mgmt.*, V. 34, No. 9-11, p. 815-821, 1993.
- Nagy, K. L., Dissolution and precipitation kinetics of sheet silicates, 1995, *Chemical Weathering Rates of Silicate Minerals*, V. 31, p. 291–351.
- Narasimhan, T. N., and Witherspoon, P. A., 1976, An integrated finite difference method for analyzing fluid flow in porous media, *Water Resources Research*, v. 12, p. 57–64.
- Nordstrom, D. K., and Muñoz, J. L., 1986, *Geochemical Thermodynamics*, The Benjamin/Cummings Pub. Co., Menlo Park, California, 477 p.
- Nordstrom, D. K., Alpers, C. N., 1997, The Environmental geochemistry of mineral deposits. Part A. Processes, methods and health issues, Plumlee, G. S., Logsdon, M. J. (Eds), *Reviews in Economic Geology*, v. 6, Society of Economic Geologists.
- Ortoleva, P. J., Dove, P., and Richter, F., 1998, Geochemical perspectives on CO₂ sequestration, Manuscript prepared for U. S. Department of Energy Workshop on “Terrestrial Sequestration of CO₂ - An Assessment of Research Needs,” Gaithersburg, MD, May 10 - 12.

- Parkhurst, D. L., Thorstenson, D. C., and Plummer, L. N., 1980, PHREEQE: A computer program for geochemical calculations: US Geological Survey, Water Resources Investigation 80-96, 174 p.
- Pearce, J. M., Holloway, S., Wacker, H., Nelis, M. K., Rochelle, C., and Bateman, K., 1996, Natural occurrences as analogues for the geological disposal of carbon dioxide. *Energy Convers. Mgmt.*, V. 37 (6-8), p. 1123-1128.
- Perkins, E. H., and Gunter, W. D., 1995, A users manual for β PATHARC.94: a reaction path-mass transfer program, Alberta Research Council Report ENVTR 95-11, 179p.
- Plummer, L. N., Wigley, T. M., and Parkhurst, D. L., 1978, The kinetics of calcite dissolution in CO₂ systems at 5°C to 60°C and 0.0 to 1.0 atm CO₂, *American Journal of Science*, v. 278, p. 179-216.
- Pruess, K., 1991, TOUGH2: A general numerical simulator for multiphase fluid and heat flow: Lawrence Berkeley Laboratory Report LBL-29400, Berkeley, California.
- Reed, M. H., 1982, Calculation of multicomponent chemical equilibria and reaction processes in systems involving minerals, gases and aqueous phase, *Geochimica et Cosmochimica Acta*, v. 46, p. 513-528.
- Rochelle, C. A., Bateman, K., and Pearce, J. M., 1996, Fluid-rock interactions resulting from the underground disposal of carbon dioxide, In Bottrell, S. H. (ed.), Proc., 4th Int. Symp. Geochem, Earth's Surf., University of Leeds, Dep. of Earth Sciences, Leeds, UK., p. 448-452.
- Ross, G. D., Todd, A. C., Tweedie J. A., and Will, A. G. S., 1982, The dissolution effects of CO₂-brine systems on the permeability of U.K. and North Sea Calcareous Sandstones, Society of Petroleum Engineers/U.S. Department of Energy Third Joint Symposium on Enhanced Oil Recovery, Paper SPE/DOE 10685, p. 149-154.
- Rudnicki, J. I., and Wawersik, W. R., 1999, Report looks at sequestering CO₂ beneath earth's surface, EOS, Transactions of American Geophysical Union, v. 80, No. 50, p. 607-608.
- Sayegh, S. G., Krause, F. F., Girard, M., and Debree, C., 1990, Rock/fluid interactions of carbonated brines in a sandstone reservoir, Pembina Cardium, Alberta, Canada, Society of Petroleum Engineers Formation Evaluation, Paper SPE19392, V. 5, p. 399-405.

- Spycher, N. F., and Reed, M. H., 1988, Fugacity coefficients of H₂, CO₂, CH₄, H₂O and of H₂O-CO₂-CH₄ mixtures: A virial equation treatment for moderate pressures and temperatures applicable to calculations of hydrothermal boiling: *Geochimica et Cosmochimica Acta*, v. 52, p. 739-749.
- Svensson, U. and Dreybrodt, W., 1992. Dissolution kinetics of natural calcite minerals in CO₂-water systems approaching calcite equilibrium.” *Chemical Geology*, v. 100, p. 129–145. Amsterdam, The Netherlands, Elsevier Science Publishers.
- Steefel, C. I., and van Cappellen, P., 1990, A new kinetic approach to modeling water-rock interaction: The role of nucleation, precursors and Ostwald ripening, *Geochimica Cosmochimica Acta*, v. 54, p. 2657-2677.
- Steefel, C. I., and Lasaga, A. C., 1994, A coupled model for transport of multiple chemical species and kinetic precipitation/dissolution reactions with applications to reactive flow in single phase hydrothermal system, *American Journal of Science*, v. 294, p. 529-592.
- Tester, J. W., Worley, G. W., Robinson, B. A., Grigsby, C. O., and Feerer, J. L., 1994, Correlating quartz dissolution kinetics in pure water from 25° to 625 °C., *Geochimica et Cosmochimica Acta*, v. 58, p. 2407–2420.
- White, A. F., and Peterson, M. L., 1990, Role of reactive surface area characterization in geochemical models, In *Chemical Models of Aqueous Systems 2*, Amer. Chem. Soc. Symp. Ser., 461-475.
- Wolery, T. J., 1992, EQ3/6: Software package for geochemical modeling of aqueous systems: Package overview and installation guide (version 7.0), Lawrence Livermore National Laboratory Report UCRL-MA-110662 PT I, Livermore, California.
- Xu, T., and Pruess, K., 1998, Coupled modeling of non-isothermal multiphase flow, solute transport and reactive chemistry in porous and fractured media: 1. Model development and validation: Lawrence Berkeley National Laboratory Report LBNL-42050, Berkeley, California, 38 p.
- Xu, T., and Pruess, K., 2000, Modeling multiphase non-isothermal fluid flow and reactive geochemical transport in variably saturated fractured rocks: 1. Methodology, *American Journal of Science*, In press.

Yeh, G. T., and Tripathi, V. S., 1991, A model for simulating transport of reactive multispecies components: model development and demonstration, *Water Resources Research*, v. 27, p. 3075-3094.